Received April 22, 2021, accepted May 10, 2021, date of publication May 17, 2021, date of current version May 25, 2021.

Digital Object Identifier 10.1109/ACCESS.2021.3081483

UAVs-UGV Leader Follower Formation Using Adaptive Non-Singular Terminal Super Twisting Sliding Mode Control

NASIM ULLAH[1], YASIR MEHMOOD[2], JAWAD ASLAM[2], AMJAD ALI[3], AND JAMSHED IQBAL[4]

[1]Department of Electrical Engineering, College of Engineering, Taif University, Taif 21974, Saudi Arabia
[2]School of Mechanical and Manufacturing Engineering, National University of Sciences and Technology, Islamabad 44000, Pakistan
[3]Department of Electrical Engineering, University of Engineering and Technology, Jalozai Campus, Peshawar 25120, Pakistan
[4]Department of Computer Science and Technology, Faculty of Science and Engineering, University of Hull, Hull HU6 7RX, U.K.

Corresponding author: Nasim Ullah (nasimullah@tu.edu.sa)

This research work was supported by Taif University Researchers Supporting Project number (TURSP-2020/144), Taif University, Taif, Saudi Arabia.

ABSTRACT Leader follower formation of unmanned aerial vehicles (UAVs) and unmanned ground vehicles (UGVs) has found numerous applications such as surveillance of critical infrastructure, industrial automation and disaster management emergency. For completion of high precision group tasks, the choice of appropriate control mechanism is of utmost importance. In presence of environmental effects,external disturbances and parametric uncertainties in the UAVs and UGV models, the controller design process is a challenging task. In order to address the aforementioned problems and to ensure minimum tracking errors and fast convergence of the states, this article proposes an adaptive robust formation and trajectory tracking control scheme for a leader follower formation of UAVs and UGV using Non-Singular Terminal Super Twisting Sliding Mode Control Method.Adaptive compensators are derived based on Lyapunov function method and stability of the proposed controllers is guaranteed. Two variants of the control schemes namely Adaptive Super Twisting SMC (AST-SMC) and Adaptive Non-Singular Terminal Super Twisting SMC (ANSTS-SMC) are tested using numerical simulations performed in MATLAB/Simulink. From the results presented, and with the proposed ANSTS-SMC control scheme, the measured $[X\ Y]$ tracking errors for leader, follower1 and follower2 UAVs are $[0\ 0.01]m$,$[0.01\ 0.02]m$ and $[0.01,\ 0.02]m$ respectively, While with the AST-SMC method the peak $[X\ Y]$ tracking errors for leader, follower1 and follower2 UAVs are $[0.05\ 0.05]m$,$[0.1\ 0.2]m$ and $[0.05\ 0.1]m$ respectively. The proposed leader follower formation can be effectively used to monitor solar/PV panels and cables in large solar parks.

INDEX TERMS Adaptive robust control, formation control, quad-rotor control, super twisting sliding mode control, solar park monitoring.

NOMENCLATURE

u, w	Linear and Angular velocities of unicycle robot respectively $[m/sec, rad/sec]$
$\ddot{X}_i, \ddot{Y}_i, \ddot{Z}_i$	Accelerations of i^{th} quad-rotor in earth coordinates $[m/sec^2]$
$\dot{X}_i, \dot{Y}_i, \dot{Z}_i$	Velocity of i^{th} quad-rotor in earth coordinates $[m/sec]$
Ω_{ri}	Overall speed of the propellers of i^{th} quad-rotor $[rad/sec]$
ϕ_i	Roll angle of i^{th} quad-rotor $[rad]$
ψ_i	Yaw angle of i^{th} quad-rotor $[rad]$
θ_i	Pitch angle of i^{th} quad-rotor $[rad]$
θ_{robot}	Unicycle robot orientation $[rad]$
D_{Xi}	Uncertainty in $\ddot{X}$ dynamics of i^{th} quad-rotor $[m/sec^2]$
$D_{xrobot}, D_{yrobot}, D_u, D_w$	Uncertainty terms in dynamics and kinematics of the unicycle robot $[m/sec^2]$

The associate editor coordinating the review of this manuscript and approving it for publication was Wei Xu.

D_{Yi}	Uncertainty in $\ddot{Y}$ dynamics of i^{th} quad-rotor $[m/sec^2]$
g	Acceleration due to gravity $[m/sec^2]$
I_{xi}, I_{yi}, I_{zi}	Moments of i^{th} quad-rotor inertia in X, Y and Z coordinates respectively $[kg-m^2]$
J_{ri}	Rotor inertia of i^{th} quad-rotor $[kg.m^2]$
$M_{\phi i}$	Roll moment of i^{th} quad-rotor $[Nm]$
$M_{\psi i}$	Yaw moment of i^{th} quad-rotor $[Nm]$
$M_{\theta i}$	Pitch moment of i^{th} quad-rotor $[Nm]$
m_{Qi}	Mass of i^{th} quad-rotor $[kg]$
X_i, Y_i, Z_i	Position of i^{th} quad-rotor in earth coordinates $[m]$
X_{robot}, Y_{robot}	Position of the unicycle robot in inertial frame $[m]$

I. INTRODUCTION

A flight in which more than one quad-rotors fly and maintain the relative distance among each other is called formation flight. In recent times, the field of unmanned aerial vehicles (UAVs) has evolved very fast. Particularly, the progress made in the formation control of unmanned autonomous vehicle have propelled the field of autonomous robots tremendously. This resulted in an increased interest in the formation control of quad-rotors. The trend is due to the numerous applications of quad-copters in defense industry, aerial mapping, search and rescue operations, oil fields monitoring, agriculture, disaster management and transportation of suspended loads [1]. The payload market value of quad-copter UAVs is expected to reach USD 3 billion by 2027 due to its anticipated usefulness [2]. The swarm of quad-rotors is advantageous due to its increased capacity for equipping sensors, support for larger payload capacity and enhanced surveillance area as compared to a single quad-rotor [3]–[7]. However, the formation control of swarm of quad-rotors in the presence of uncertainties is a very difficult task. Moreover, formation dynamic model of swarm of UAVs in the presence of external disturbances has also become an important topic.

The translational and rotational dynamics of a quad-rotor is modeled as six degree of freedom nonlinear differential equations [8]–[11]. Different formation geometries exist for multiple quad-copters depending upon the number of quad-rotors and the purpose of flight. Two of them are V shape geometry and finger four geometry. In this paper, a V shaped geometry is used for the flight formation of 3 quad-rotors for the purpose of demonstration. The formation of the quad-copters can be stepped up, stepped down and leveled depending upon the altitude position between leader and follower. Leveled formation of quad-copters is used in this paper. The system of quad-rotor is an under-actuated multi-variable non-linear model making the system dynamics complex thus requiring a sophisticated formation trajectory control law. The uncertainties in the model and those produced due to wind gust must be compensated using appropriate control schemes in order to ensure robust formation control of quad-copters.

To ensure the robustness of quad-copter in the presence of disturbances and to solve the problem of formation control of multiple quad-rotors, many research efforts have been made. Abbas *et al.* presented a leader–follower formation controller using classical proportional derivative scheme for tracking of leader on the desired trajectory and fuzzy logic system in order to achieve the desired formation pattern [12]. However, the uncertainties in the above controller were not taken into consideration. In [13], a finite time control scheme and a prescribed performance controller is presented for leader-follower formation control of group of quad-copters. The presented performance controller controls the translational movements and desired orientations while the finite-time formation controller makes the followers to track the desired path. In the work of Wua *et al.* [14], each single quad-rotor is controlled by a linear Proportional-Integral-Derivative (PID) controller and the formation flying problem is solved by adopting a sliding mode controller (SMC). However the disturbances and communication delays between multiple UAVs is ignored in the above mentioned PID-SMC based scheme.

The formation control problem of group of quad-rotors is solved using classical SMC technique in [15]–[17], however high frequency chattering is produced in the excitation signal in the classical SMC method thereby reducing the life of the actuators. Abas *et al.* in [18] presents a circular leader-follower formation control scheme for multiple aerial vehicles. A synchronized position tracking PI controller for the formation control of two UAVs is presented in [19]. Abdessameud *et al.* presented a distributed control algorithm to achieve a desired formation pattern and to compensate the communication delays in multiple UAVs formation [20]. In order to control the formation of micro UAVs, a nonlinear distributed controller is proposed in [21]. In the work of Bayezit *et al.*, a distributed cohesive motion controller is proposed for the formation of multiple UAVs [22]. A distributed back-stepping controller is designed for the formation control problem of swarm of UAVs in [23]. Similarly, a non-linear model predictive controller which is tuned using adaptive gain method is proposed for the trajectory control of multiple UAVs in [24], [25]. Wang *et al.* proposed a priori-bounded intermediary adaptive controller for the velocity tracking and formation control of quad-rotors which gives the reference orientation and bounded control thrust [26].

For the formation control of quad-rotors with attached slung load, a Lyapunov function based guidance algorithm is used, with a linear quadratic tracking controller [27]. Rifqi *et al.* implement a Leader-follower formation controller for two parrot AR drones, where a dedicated PD controller is designed for the respective models [28]. A distance based formation controller is designed for the formation and tracking

control of quad-rotors in leader-follower formation which has the capabilities of collision avoidance via Lyapunov barrier functions [29]. A classical adaptive controller is designed for the formation control of swarm of UAVs in leader follower formation in an environment with motion constraints and unknown external disturbances [30]. Estévez *et al.* proposed a model reference adaptive control for multiple quad-rotors [31]. This controller uses fuzzy modeling of the error to regulate the activation of the adaptation rules applied to PD controller parameters. These rules are derived as error gradient descent rules. A semi-physical platform for multiple fixed winged UAVs to control its formation is proposed in [33]. In [34], a detailed survey on inexpensive UAV platforms for infrastructure inspection is presented.

The above cited work is specifically focused on the formation control of multiple UAVs. It is also necessary to describe the background of robust control system due to its utmost importance in control community. Fari proposed a robust adaptive vector field controller for compensating unmodelled dynamics of a UAV [35], [36]. Robust controllers are designed both in frequency and time domains. A widely utilized frequency domain robust controller is the H_∞ method. Several variants of H_∞ control were reported in the literature. Some of them include the loop shaping method which is discussed in [36], optimal H_∞ control using Riccati equations in [37] and Linear Matrix Inequalities (LMIs) based design of the controller in [38]. In the book of Edwards *et al.*, sliding mode control (SMC) theory is discussed to overcome the discrepancies between actual plant and mathematical model for controller design [39]. Classical SMC has several disadvantages such as high frequency chattering and asymptotic convergence property [40]. These disadvantages are addressed by the introduction of new variants of slide mode controllers such as Linear Matrix Inequalities based SMC [41], Higher order sliding mode controller [42], [43], Lyapunov function based adaptive SMC and Non singular terminal SMC in [44]. The stability of the SMC controllers is ensured by Lyapunov theorem [45]. Tripathi *et al.* proposed a non-linear fast terminal sliding mode super twisting controller (FTSMSTC) design for quad-rotor position and altitude tracking in the presence of bounded disturbances [46]. For the fast convergence of tracking error to zero and to avoid singularity problem, a nonlinear fast terminal SMC has been proposed in the above work. In the research work of Feng *et al.*, a method is proposed to overcome the singularity problem that arises in terminal SMC [47]. A global non-singular terminal SMC strategy has been developed for non-linear systems which ensures the finite time convergence of the system to the sliding surface. An incremental non-singular terminal SMC for MIMO systems having model uncertainties and external perturbations is proposed in [48]. Chattering free attitude tracking of quad-copters is achieved by non-singular terminal SMC in [49]. The proposed theorems ensure global stability of the nonlinear systems and control given the condition that the disturbances are bounded.

From the above cited literature, several research challenges have been identified for the formation control problem of swarm of UAVs and it include the lack of knowledge of the wind vector, unmodeled course angle dynamics, uncertain course time constant, state-dependent uncertainty in the course dynamics arising from coupling and collision avoidance due to sling loads [27], [35], [36], [51].

Considering the aforementioned literature review, this paper proposes adaptive robust formation and trajectory tracking of leader-follower UAVs and UGVs using non-singular terminal super-twisting SMC method. Since Non singular terminal SMC method ensures finite time convergence of the states, while super twisting SMC minimizes the chattering phenomena, thus both of the mentioned methods are combined to utilize their advantages in one hybrid controller. The proposed controller compensates the disturbances using adaptive control laws derived by Lyapunov function method. System stability is ensured using Lyapunov theorem. Furthermore, the formation flight between multiple UAVs and UGVs is also controlled using non-singular terminal super-twisting SMC methods.

The rest of the paper is organized into four sections. Section 2 is related to system description and mathematical modeling. The objective of this section is the modelling of a single quad-rotor and transnational dynamics of multiple UAVs. Section 3 formulates the trajectory and the formation controller for UAVs and UGVs vehicles. In section 4, the simulation results are presented with a comparative analysis for different controllers. Finally, Section 5 comments on the conclusions. Following specific contributions are highlighted:

1. In presence of external disturbances, robust formation and trajectory tracking of multiple UAVs and UGVs is achieved using non singular terminal super-twisting sliding mode control method.

2. The adaptive laws are derived using Lyapunov theorem and implemented using projection operators.

II. SYSTEM DESCRIPTION AND MATHEMATICAL MODELING

Fig. 1 shows the potential application of UAVs and UGV leader-follower formation. As shown, the aerial UAVs can be utilized for solar panel health monitoring and UGV ground vehicle is utilized for cable inspection. In this work, we are only focused on the trajectory and formation control of UAVs and UGV while the sensors and algorithms for health monitoring of the solar panels and cables are excluded. Before deriving formation and trajectory controllers, it is necessary to formulate the mathematical model of a quad-rotor UAV in earth's reference coordinates (X, Y, Z). Apart from inertial frame of reference, the body coordinates of the UAV are given as: (X_B, Y_B, Z_B). To derive the model, the following assumptions are made.

Assumption 1: UAVs are represented by a symmetrical rigid body configurations with masses m.

Assumption 2: The external disturbances affect the X and Y accelerations components of each UAV.

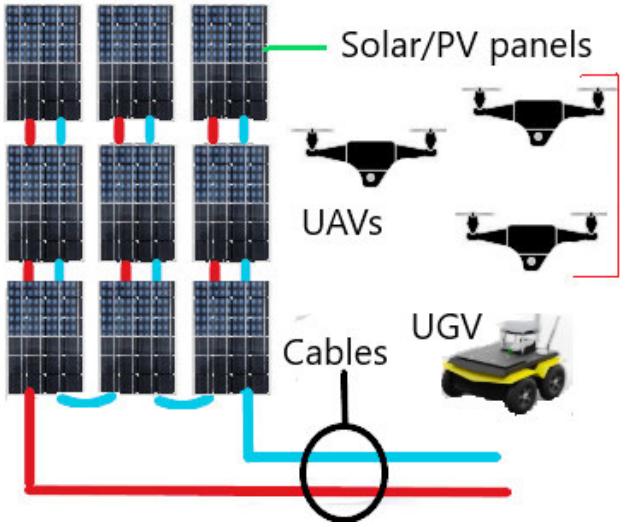

FIGURE 1. Solar panels and cables health monitoring using drones.

Assumption 3: The disturbances are uniformly affecting the leader and followers. Figure 2a shows the vector diagram of multiple UAV quad-rotors in leader follower configuration. Based on the above assumptions, the dynamic model of the multiple UAV quad-rotors is formulated as 6 degree of freedom equations. The equations expressing the linear and angular dynamics of the quad-rotors are given as follows:

$$\ddot{X}_i = (\sin\psi_i \sin\phi_i + \cos\psi_i \sin\theta_i \cos\phi_i)\frac{U_{1i}}{m_{Qi}} - D_{Xi} \quad (1)$$

$$\ddot{Y}_i = (-\cos\psi_i \sin\phi_i + \sin\psi_i \sin\theta_i \cos\phi_i)\frac{U_{1i}}{m_{Qi}} - D_{Yi} \quad (2)$$

$$\ddot{Z}_i = g - (\cos\theta_i \cos\phi_i)\frac{U_{1i}}{m_{Qi}} - D_{Zi} \quad (3)$$

$$\ddot{\phi}_i = \frac{I_{yi} - I_{zi}}{I_{xi}}\dot{\theta}_i\dot{\psi}_i - \frac{J_{ri}}{I_{xi}}\dot{\theta}_i\Omega_{ri} + \frac{l_i}{I_{xi}}U_{2i} - D_{\phi_i} \quad (4)$$

$$\ddot{\theta}_i = \frac{I_{zi} - I_{xi}}{I_{yi}}\dot{\phi}_i\dot{\psi}_i - \frac{J_{ri}}{I_{yi}}\dot{\phi}_i\Omega_{ri} + \frac{l_i}{I_{yi}}U_{3i} - D_{\theta_i} \quad (5)$$

$$\ddot{\psi}_i = \frac{I_{xi} - I_{yi}}{I_{zi}}\dot{\phi}_i\dot{\theta}_i + \frac{l_i}{I_{zi}}U_{4i} - D_{\psi_i} \quad (6)$$

Equation (1-6) formulate the mathematical model of multiple quad-rotors UAV. In (1-6), D_{Xi} and D_{Yi} represent the uncertainty in X and Y acceleration channels respectively, while i is an index representing $[L,\ j]$ and $j = [F_1, F_2, F_3]$. The subscript L represents the leader UAV, while F_1 and F_2 show follower 1 and 2 aerial UAVs respectively. Moreover F_3 represents follower 3 ground robot.

Referring to Fig. 2, the translational dynamics of the UAVs is expressed as follows:

$$\dot{X}_i = V_{Xi}\cos(\psi_i) - V_{Yi}\sin(\psi_i) \quad (7)$$

$$\dot{Y}_i = V_{Xi}\sin(\psi_i) + V_{Yi}\cos(\psi_i) \quad (8)$$

$$\dot{\psi}_L = \omega_L \quad (9)$$

where V_{Xi} and V_{Yi} represent the velocities in X and Y directions of the inertial frame respectively. As shown in Fig. 2, let the follower UAVs maintain d_{Xj} and d_{Yj} distances in X and Y planes respectively with respect to the leader UAV, so d_{Xj} and d_{Yj} are expressed as follows:

$$d_{Xj} = -(X_L - X_j)\cos(\psi_L) - (Y_L - Y_j)\sin(\psi_L) \quad (10)$$

$$d_{Yj} = (X_L - X_j)\sin(\psi_L) - (Y_L - Y_j)\cos(\psi_L) \quad (11)$$

where $d_{Xj} = d_i cos(\phi)$, $d_{Yj} = d_i sin(\phi)$ and $X_j = [X_{F1},\ X_{F2},\ X_{F3}]$. The error in ψ dynamics is defined as: $e_\psi = \psi_j - \psi_L$. By taking the first derivatives of equation (10-11) with respect to time and combining the resultant expressions with equations (7-8) yields:

$$\dot{d}_{Xj} = d_{Yj}\omega_L + V_{Xj}\cos(e_\psi) - V_{Yj}\sin(e_\psi) - V_{XL} \quad (12)$$

$$\dot{d}_{Yj} = -d_{Xj}\omega_L + V_{Xj}\sin e_\psi + V_{Yj}\cos e_\psi - V_{YL} \quad (13)$$

where V_{Xj}, V_{Yj}, V_{XL} and V_{YL} represent the longitudinal and lateral velocities of the follower 1, follower 2 and leader UAVs respectively. By defining errors in the longitudinal and lateral dynamics of (12-13), the error state equation is given as:

$$\dot{\chi} = F(\chi) + G(\chi)v \quad (14)$$

Equation 14 is explained as follows:

$$\chi = \begin{bmatrix} e_{Xj} \\ e_{Yj} \\ e_\psi \end{bmatrix};\ \dot{\chi} = \begin{bmatrix} \dot{e}_{Xj} \\ \dot{e}_{Yj} \\ \dot{e}_\psi \end{bmatrix};\ v = \begin{bmatrix} V_{Xj} \\ V_{Yj} \\ \omega_F \end{bmatrix} \quad (15)$$

The terms $G(\chi)$ and $F(\chi)$ in (14) are expressed as follows:

$$F(\chi) = \begin{bmatrix} e_{Yj}\omega_L + V_{XL} - \omega_L {d_{Yj}}^d \\ -e_{Xj}\omega_L + V_{YL} + \omega_L {d_{Xj}}^d \\ e_\psi \end{bmatrix} \quad (16)$$

$$G(\chi) = \begin{bmatrix} -ce_\psi & se_\psi & 0 \\ -se_\psi & -ce_\psi & 0 \\ 0 & 0 & 1 \end{bmatrix} \quad (17)$$

In (17), e_ψ is already defined, while c and s represent cos and sin functions respectively. Also form (15), we define: $e_{Xj} = {d_{Xj}}^d - d_{Xj}$ and $e_{Yj} = {d_{Yj}}^d - d_{Yj}$. Where ${d_{Xj}}^d$ and ${d_{Yj}}^d$ represent the desired commands. Finally the desired reference trajectories for follower UAVs and ground robot are expressed as follows:

$$X_{dj} = X_L - d_{Xj}\cos(\psi_L) - d_{Yj}\sin(\psi_L)$$

$$Y_{dj} = Y_L + d_{Xj}\sin(\psi_L) + d_{Yj}\cos(\psi_L) \quad (18)$$

III. TRAJECTORY AND FORMATION CONTROLLERS FORMULATION

In this section, firstly the derivations of the attitude, altitude and position controllers are formulated for the leader UAV. Secondly, the formation controller is derived and based on it, new references are calculated for follower 1 and follower 2 UAVs. Finally, the trajectory and attitude controllers of the leader UAV are generalized for follower UAVs. Before

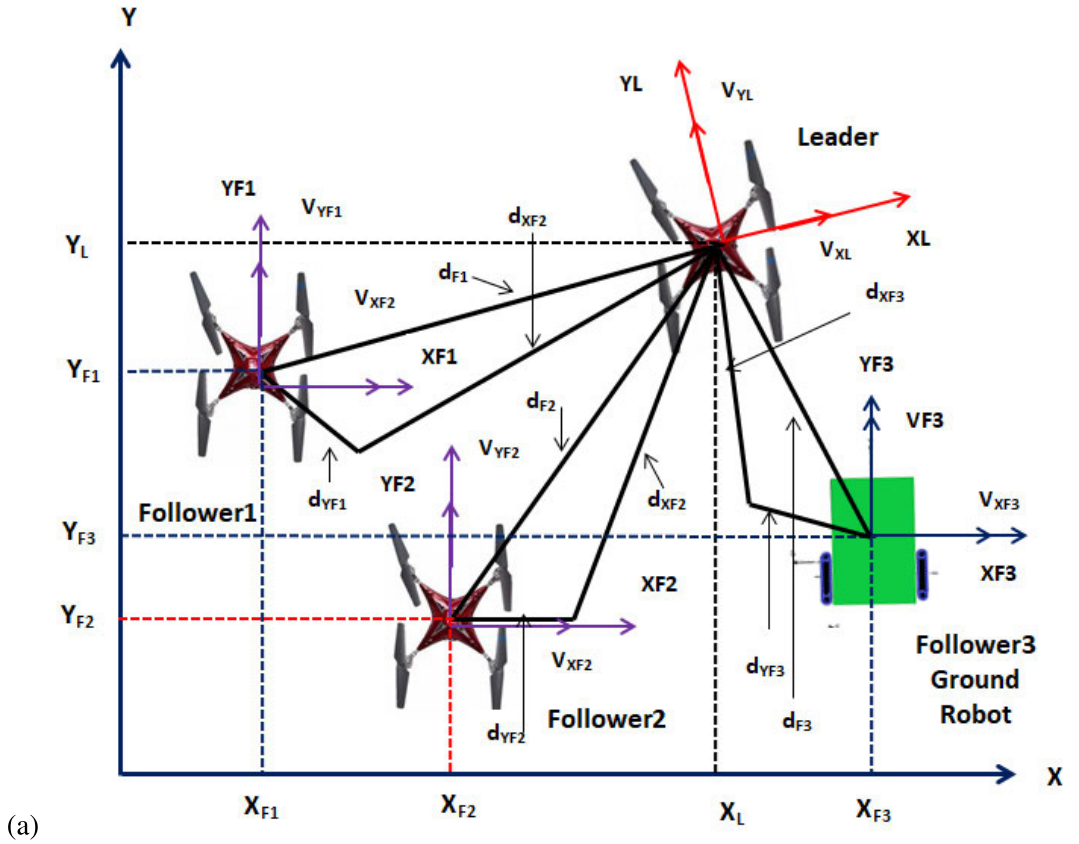

(a)

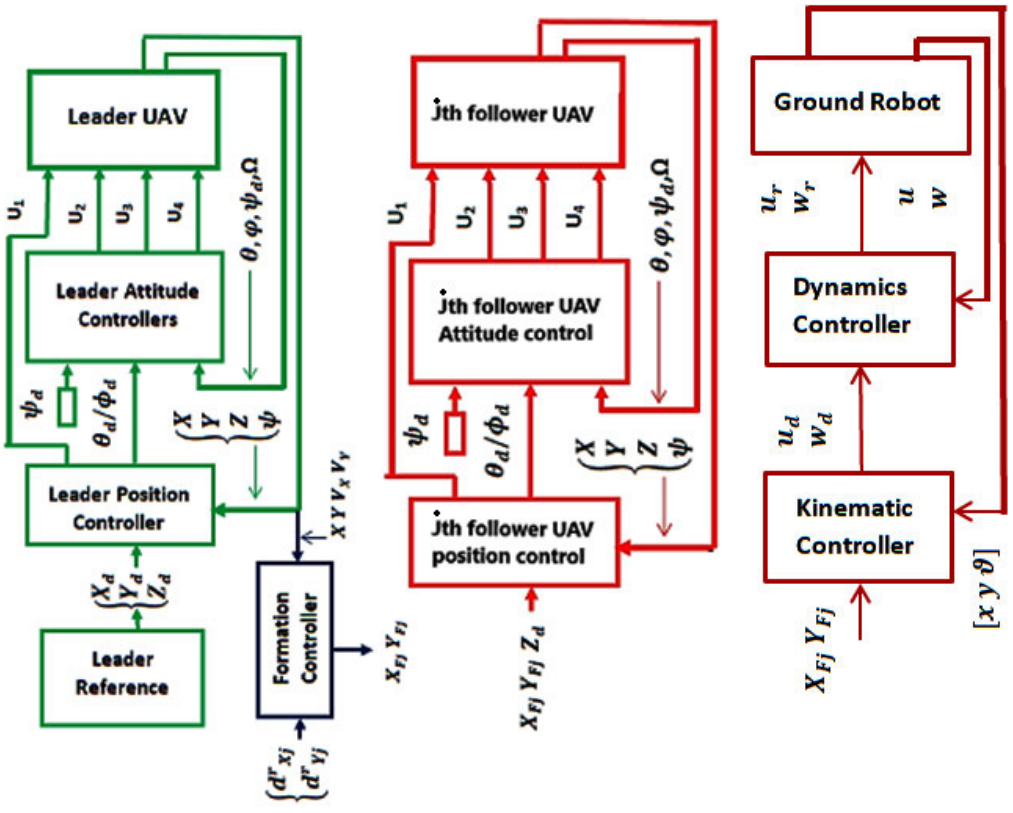

(b)

FIGURE 2. (a) Leader-follower configuration (b) Block diagram of leader-follower configuration.

deriving the control schemes, the following assumptions are made:

Assumption 4: The following condition is true for the uncertainty terms:

$||D_{Xi}|| \leq \Delta_{1i}$; $||D_{Yi}|| \leq \Delta_{2i}$;$||D_{Zi}|| \leq \Delta_{3i}$;$||D_{\phi_i}|| \leq \Delta_{4i}$;$||D_{\theta_i}|| \leq \Delta_{5i}$;$||D_{\psi_i}|| \leq \Delta_{6i}$

where Δ_{1i}, Δ_{2i},Δ_{3i},Δ_{4i},Δ_{5i},Δ_{6i} represent the upper bound of the mentioned uncertainties.

A. LEADER UAV CONTROL FORMULATION

In this subsection, the attitude, altitude and position controllers are derived for leader UAV using adaptive super twisting terminal SMC method.

1) ATTITUDE CONTROL

Attitude controllers regulate the roll, yaw and pitch angles of the UAV. Let the reference Euler angle commands for the leader UAV are set as $\phi_{dL}, \theta_{dL,}\psi_{dL}$, then the desired sliding manifold is chosen as follows:

$$S_{\phi_L} = k_1 e_{\phi_L} + k_2 \dot{e}_{\phi_L} + k_{21} e_{\phi_L}^{\gamma_{\phi_L}} \tag{19}$$

where S_{ϕ_L} represents the sliding surface for ϕ_L loop, k_1, k_2 and k_{21} are the design constants and the ϕ_L loop error dynamics is expressed as follows: $e_{\phi_L} = \phi_L - \phi_{dL}$, $\dot{e}_{\phi_L} = \dot{\phi}_L - \dot{\phi}_{dL}$. By taking the first time derivative of (19), the following expression is obtained:

$$\dot{S_{\phi_L}} = k_1 \dot{e_{\phi_L}} + k_2 \ddot{e_{\phi_L}} + k_{21}\gamma_{\phi_L} e_{\phi_L}^{\gamma_{\phi_L}-1}\dot{e}_{\phi_L} \tag{20}$$

Equation (4) and Equation (20) are combined and expressed as follows:

$$\begin{aligned}\dot{S_{\phi_L}} = {} & k_1 \dot{e_{\phi_L}} + k_{21}\gamma_{\phi_L} e_{\phi_L}^{\gamma_{\phi_L}-1}\dot{e}_{\phi_L} + k_2[a_{1L}\dot{\theta}_L\dot{\psi}_L \\ & - a_{2L}\dot{\theta}_L\Omega_{rL} + b_{1L}U_{2L} - D_{\phi_L} - \ddot{\phi}_{dL}]\end{aligned} \tag{21}$$

In (21), the coefficients are defined as follows: $a_{1L} = \frac{I_{yL}-I_{zL}}{I_{xL}}$, $a_{2L} = \frac{J_{rL}}{I_{xL}}$, $b_{1L} = \frac{l}{I_{xL}}$; then the equivalent control law for ϕ_L loop is derived as follows:

$$\begin{aligned}U_{2Leq} = \frac{1}{b_{1L}}\Bigg(-\frac{k_1}{k_2}\dot{e_{\phi_L}} - \frac{k_{21}}{k_2}\gamma_{\phi_L} e_{\phi_L}^{\gamma_{\phi_L}-1}\dot{e}_{\phi_L} - a_{1L}\dot{\theta}_L\dot{\psi}_L \\ + a_{2L}\dot{\theta}_L\Omega_{rL} + \ddot{\phi}_{dL}\Bigg)\end{aligned} \tag{22}$$

Using super twisting algorithm, the switching control law is derived as follows:

$$U_{2Lsw} = \frac{-k_{d1}}{b_{1L}}|S_{\phi_L}|^{0.5}sgn(S_{\phi_L}) - \frac{k_{d2}}{b_{1L}}\int sgn(S_{\phi_L}) \tag{23}$$

Referring to (22) and (23), the total control action is the sum of equivalent and switching control parts i.e. $U_{2L} = U_{2Leq} + U_{2Lsw}$. Similar procedure is adopted to derive the pitch and yaw controllers. The sliding surfaces for θ_L and ψ_L loops are defined as follows: $S_{\theta_L} = k_3 e_{\theta_L} + k_4 \dot{e}_{\theta_L} + k_{34} e_{\theta_L}^{\gamma_{\theta_L}}$ and $S_{\psi_L} = k_5 e_{\psi_L} + k_6 \dot{e}_{\psi_L} + k_{56} e_{\psi_L}^{\gamma_{\psi_L}}$, then the θ_L and ψ_L loops controllers are formulated as follows:

$$\begin{aligned}U_{3Leq} = \frac{1}{b_{2L}}\Bigg(\frac{-k_3}{k_4}\dot{e_{\theta_L}} - \frac{k_{34}}{k_4}\gamma_{\theta_L} e_{\theta_L}^{\gamma_{\theta_L}-1}\dot{e}_{\theta_L} - a_{3L}\dot{\phi}_L\dot{\psi}_L \\ + a_{4L}\dot{\phi}_L\Omega_{rL} + \ddot{\theta}_{dL}\Bigg)\end{aligned} \tag{24}$$

$$U_{3Lsw} = \frac{-k_{d3}}{b_{2L}}|S_{\theta_L}|^{0.5}sgn(S_{\theta_L}) - \frac{k_{d4}}{b_{2L}}\int sgn(S_{\theta_L}) \tag{25}$$

$$\begin{aligned}U_{4Leq} = \frac{1}{b_{3L}}\Bigg(\frac{-k_5}{k_6}\dot{e_{\psi_L}} - \frac{k_{56}}{k_6}\gamma_{\psi_L} e_{\psi_L}^{\gamma_{\psi_L}-1}\dot{e}_{\psi_L} \\ - a_{5L}\dot{\phi}_L\dot{\theta}_L + \ddot{\psi}_{dL}\Bigg)\end{aligned} \tag{26}$$

$$U_{4Lsw} = \frac{-k_{d5}}{b_{3L}}|S_{\psi_L}|^{0.5}sgn(S_{\psi_L}) - \frac{k_{d6}}{b_{3L}}\int sgn(S_{\psi_L}) \tag{27}$$

In (19-27), constant parameters $k_1, k_2, k_3, k_4, k_5, k_6$, $k_{12}, k_{34}, k_{56}, \gamma_{\phi_L}, \gamma_{\theta_L}, \gamma_{\psi_L}, k_{d1}, k_{d2}, k_{d3}, k_{d4}, k_{d5}, k_{d6}$ represent the gains of the controllers and the sliding surface. The coefficients are defined as follows:$a_{3L} = \frac{I_{zL}-I_{xL}}{I_{yL}}$, $a_{4L} = \frac{J_{rL}}{I_{yL}}$, $b_{2L} = \frac{lL}{I_{yL}}$, $a_{5L} = \frac{I_{xL}-I_{yL}}{I_{zL}}$ and $b_{3L} = \frac{lL}{I_{xL}}$, Moreover S_{θ_L} and S_{ψ_L} represent the sliding surfaces for θ_L and ψ_L loops respectively. The corresponding error dynamics for θ_L and ψ_L loops are expressed as follows: $e_{\theta_L} = \theta_L - \theta_{dL}$, $\dot{e}_{\theta_L} = \dot{\theta}_L - \dot{\theta}_{dL}$, $e_{\psi_L} = \psi_L - \psi_{dL}$, $\dot{e}_{\psi_L} = \dot{\psi}_L - \dot{\psi}_{dL}$.

Theorem 1: Consider the nonlinear system presented in (4-6),satisfying assumptions 1-3, then under the proposed controllers of (22-23) and (24-25), the states of the attitude dynamics will converge to the origin in finite time.

Proof of Theorem 1: The stability proof is only derived for ϕ_L loop only. Similar procedures can be adopted for the other two loops of attitude dynamics. Equation (23) is modified as follows: $U_{2Lsw} = \frac{-k_{d1}}{b_{1L}}|S_{\phi_L}|^{0.5}sgn(S_{\phi_L}) + v_{\phi L}$; where the term $v_{\phi L}$ is calculated from the following expression: $\dot{v}_{\phi L} = \frac{k_{d2}}{b_{1L}}sgn(S_{\phi_L})$. By combining the above terms with (21-22), $\dot{S}_{\phi L}$ is expressed as follows:

$$\begin{aligned}\dot{S_{\phi_L}} &= \frac{-k_{d1}}{b_{1L}}|S_{\phi_L}|^{0.5}sgn(S_{\phi_L}) + v_{\phi L} - D_{\phi L} \\ \dot{v}_{\phi L} &= -\frac{k_{d2}}{b_{1L}}sgn(S_{\phi_L})\end{aligned} \tag{28}$$

Let the Lyapunov function for ϕ loop dynamics is chosen as follows: $V_{\phi_L} = 2\tau_2|S_{\phi_L}| + 0.5v_{\phi L}^2 + 0.5[\tau_1|S_{\phi_L}|^{0.5}sgn(S_{\phi_L}) - v_{\phi L}]^2$. Where $\tau_1 = \frac{k_{d1}}{b_{1L}}$ and $\tau_2 = \frac{k_{d2}}{b_{1L}}$. A new state vector is defined as follows: $\eta_{\phi L}^T = [|S_{\phi_L}|^{0.5}sgn(S_{\phi_L})\ v_{\phi L}]$. Define matrix $P_{\phi L} = \begin{bmatrix}4\tau_2+\tau^2 & -\tau_1 \\ -\tau_1 & 2\end{bmatrix}$ and then the Lyapunov function is expressed as follows: $V_{\phi_L} = \eta_{\phi L}^T P \eta_{\phi L}$ The time derivative of the Lyapunov function along (28) yields the following relation [32]:

$$\dot{V_{\phi_L}} = -\frac{1}{\left|S_{\phi_L}^{0.5}\right|}\eta_{\phi L}^T Q \eta_{\phi L} + \Delta_{4L} q_{\phi L}^T \eta_{\phi L} \tag{29}$$

where the new matrices are represented as follows: $Q_{\phi L} = \frac{\tau_1}{2}\begin{pmatrix}2\tau_2+\tau_1^2 & -\tau_1 \\ -\tau_1 & 1\end{pmatrix}$ and $q_{\phi L}^T = \left(2\tau_2 + \frac{1}{2}\tau_1^2 - \frac{1}{2}\tau_1\right)$. Applying the uncertainty bounds mentioned in Assumption 4, expression (29) is simplified as follows [32]:

$$\dot{V_{\phi L}} = -\frac{\tau_1}{2\left|S_{\phi L}^{0.5}\right|}\eta_{\phi L}^T \tilde{Q_{\phi L}} \eta_{\phi L} \tag{30}$$

where matrix $\tilde{Q_{\phi L}}$ is:

$$\tilde{Q_{\phi L}} = \begin{pmatrix} 2\tau_2 + \tau_1^2 - \left(\frac{4\tau_2}{\tau_1} + \tau_1\right)\Delta_{4L} & -\tau_1 + 2\Delta_{4L} \\ -\tau_1 + 2\Delta_{4L} & 1 \end{pmatrix}.$$

Equation (30) is negative definite only if $\tilde{Q_{\phi L}} > 0$. If the gains satisfy the following criteria $\tau_1 > 2\Delta_{4L}$, $\tau_2 > \tau_1 \frac{5\Delta_{4L}\tau_1 + 4\Delta_{4L}^2}{2(\tau_1 - 2\Delta_{4L})}$, then $\tilde{Q} > 0$ and $\dot{V}_{\phi_L} < 0$.

Remark1: The proof of finite time convergence property can be derived by using the procedures adopted in [32].

2) ALTITUDE AND POSITION CONTROL

This section formulates the altitude and position control system for the leader UAV expressed in (1-6). First, the altitude control system is derived and then using the transformation matrix, the position controllers are formulated. With the desired altitude Z_{dL}, the sliding manifold is written as follows:

$$S_{Z_L} = k_7 e_{Z_L} + k_8 \dot{e}_{Z_L} + k_{78} e_{Z_L}^{\gamma_{Z_L}} \tag{31}$$

In (31), k_7 and k_8 represent the design constants. The error dynamics is defined as follows: i.e. $e_{Z_L} = Z_L - Z_{d_L}$, $\dot{e}_{Z_L} = \dot{Z}_L - \dot{Z}_{Ld_L}$. Taking the first derivative of (32) w.r.t. time yields the following expression:

$$\dot{S_{Z_L}} = k_7 \dot{e_{Z_L}} + k_8 \ddot{e}_{Z_L} + k_{78}\gamma_{Z_L} e_{Z_L}^{\gamma_{Z_L}-1} \dot{e}_{Z_L} \tag{32}$$

Equation (32) and (3) are combined and expressed as follows:

$$\begin{aligned} \dot{S_{Z_L}} = {} & k_7 \dot{e_{Z_L}} + k_{78}\gamma_{Z_L} e_{Z_L}^{\gamma_{Z_L}-1} \dot{e}_{Z_L} \\ & + k_8[g - \cos\theta_L \cos\phi_L \frac{U_{1L}}{m_{QL}} - D_{ZL} - \ddot{Z}_{dL}] \end{aligned} \tag{33}$$

Using super twisting sliding mode theory, the altitude controller is derived as follows:

$$\begin{aligned} U_{Z_L} = {} & -\frac{k_7}{k_8}\dot{e_{Z_L}} - \frac{k_{78}}{k_8}\gamma_{Z_L} e_{Z_L}^{\gamma_{Z_L}-1}\dot{e}_{Z_L} + \ddot{Z_{dL}} \\ & - \frac{k_{d7}}{k_8}|S_{Z_L}|^{0.5} sgn(S_{Z_L}) - \frac{k_{d8}}{k_8}\int sgn(S_{Z_L}) \\ U_{1L} = {} & \frac{m_{QL}}{\cos\theta_L \cos\phi_L}[g - (-\frac{k_7}{k_8}\dot{e_{Z_L}} - \frac{k_{78}}{k_8}\gamma_{Z_L} e_{Z_L}^{\gamma_{Z_L}-1}\dot{e}_{Z_L} \\ & + \ddot{Z_{dL}} - \frac{k_{d7}}{k_8}|S_{Z_L}|^{0.5} sgn(S_{Z_L}) \\ & - \frac{k_{d8}}{k_8}\int sgn(S_{Z_L}))] \end{aligned} \tag{34}$$

Here $U_{Z_L} = \ddot{Z_L} = g - (\cos\theta_L \cos\phi_L)\frac{U_{1L}}{m_{QL}}$ represents the virtual control law. The stability proof is derived based on the same concepts presented for ϕ loop. The robust terms of equation (34) are modified as follows: $U_{1Lsw} = \frac{-k_{d7}}{k_8}|S_{Z_L}|^{0.5} sgn(S_{Z_L}) + v_{Z_L}$; where the term v_{Z_L} is calculated from the following expression: $\dot{v}_{Z_L} = -\frac{k_{d8}}{k_8} sgn(S_{Z_L})$. By combining the above terms with (33) and robust term of (34), $\dot{S}_{ZL}$ is expressed as follows:

$$\dot{S_{Z_L}} = \frac{-k_{d7}}{k_8}|S_{Z_L}|^{0.5} sgn(S_{Z_L}) + v_{Z_L} - D_{ZL}$$

$$\dot{v}_{Z_L} = -\frac{k_{d8}}{k_8} sgn(S_{Z_L}) \tag{35}$$

Let the Lyapunov function for Z loop is chosen as follows: $V_{Z_L} = 2\tau_8|S_{Z_L}| + 0.5v_{Z_L}^2 + 0.5(\tau_7|S_{Z_L}|^{0.5} sgn(S_{Z_L}) - v_{Z_L})^2$. Where $\tau_7 = \frac{k_{d7}}{k_8}$ and $\tau_8 = \frac{k_{d8}}{k_8}$. A new state vector is defined as follows: $\eta_{ZL}^T = [|S_{Z_L}|^{0.5} sgn(S_{Z_L}) \;\; v_{Z_L}]$. Define matrix $P_{ZL} = \begin{bmatrix} 4\tau_8 + \tau_7^2 & -\tau_7 \\ -\tau_7 & 2 \end{bmatrix}$ and then the Lyapunov function is expressed as follows: $V_{Z_L} = \eta_{ZL}^T P_{ZL} \eta_{ZL}$. The time derivative of the Lyapunov function along (35) yields the following relation:

$$\dot{V_{Z_L}} = -\frac{1}{\left|S_{Z_L}^{0.5}\right|}\eta_{ZL}^T Q_{ZL} \eta_{ZL} + \Delta_{3L} q_{ZL}^T \eta_{ZL} \tag{36}$$

where the new matrices are represented as follows: $Q_{ZL} = \frac{\tau_7}{2}\begin{pmatrix} 2\tau_8 + \tau_7^2 & -\tau_7 \\ -\tau_7 & 1 \end{pmatrix}$ and $q_{ZL}^T = \left(2\tau_8 + \frac{1}{2}\tau_7^2 - \frac{1}{2}\tau_7\right)$. Applying the uncertainty bounds given in assumption 4, expression (36) is simplified as follows:

$$\dot{V_{ZL}} = -\frac{\tau_7}{2\left|S_{ZL}^{0.5}\right|}\eta_{ZL}^T \tilde{Q_{ZL}} \eta_{ZL} \tag{37}$$

where matrix $\tilde{Q_{ZL}}$ is:

$$\tilde{Q_{ZL}} = \begin{pmatrix} 2\tau_8 + \tau_7^2 - \left(\frac{4\tau_8}{\tau_7} + \tau_7\right)\Delta_{3L} & -\tau_7 + 2\Delta_{3L} \\ -\tau_7 + 2\Delta_{3L} & 1 \end{pmatrix}$$

Equation (37) is negative definite only if $\tilde{Q_{ZL}} > 0$. If the gains satisfy the following criteria $\tau_7 > 2\Delta_{3L}$, $\tau_8 > \tau_7 \frac{5\Delta_{3L}\tau_7 + 4\Delta_{3L}^2}{2(\tau_7 - 2\Delta_{3L})}$, then $\tilde{Q_{ZL}} > 0$ and $\dot{V}_{Z_L} < 0$.

Now to derive the XY controllers, we assume the following:

$$\begin{aligned} U_{XL} &= (\sin\psi_L \sin\phi_L + \cos\psi_L \sin\theta_L \cos\phi_L)\frac{U_{1L}}{m_{QL}} \\ U_{YL} &= (-\cos\psi_L \sin\phi_L + \sin\psi_L \sin\theta_L \cos\phi_L)\frac{U_{1L}}{m_{QL}}. \end{aligned}$$

With these expressions, (1) and (2) are re-written for leader UAV in the following form:

$$\ddot{X_L} = U_{XL} - D_{XL} \tag{38}$$

$$\ddot{Y_L} = U_{YL} - D_{YL} \tag{39}$$

Let the sliding manifolds for the position loops of leader UAV are expressed as follows:

$$\begin{cases} S_{X_L} = k_9 e_{X_L} + k_{10}\dot{e}_{X_L} + k_{91}\gamma_{X_L} e_{X_L}^{\gamma_{X_L}-1}\dot{e}_{X_L} \\ S_{Y_L} = k_{11} e_{Y_L} + k_{12}\dot{e}_{Y_L} + k_{92}\gamma_{Y_L} e_{Y_L}^{\gamma_{Y_L}-1}\dot{e}_{Y_L} \end{cases} \tag{40}$$

In (40), k_9,k_{10},k_{11},k_{12} are the design constants and the error dynamics is expressed as follows: $e_{X_L} = X_L - X_{dL}$, $\dot{e}_{X_L} = \dot{X}_L - \dot{X}_{dL}$, $e_{Y_L} = Y_L - Y_{dL}$, $\dot{e}_{Y_L} = \dot{Y}_L - \dot{Y}_{dL}$. By taking the derivative of (40) w.r.t. time and combining it with (38) and (39), one acquires the following expressions:

$$\begin{cases} \dot{S_{X_L}} = k_9 \dot{e_{X_L}} + k_{91}\gamma_{X_L} e_{X_L}^{\gamma_{X_L}-1}\dot{e}_{X_L} + k_{10}[U_{XL} \\ \qquad - D_{XL} - \ddot{X}_{dL}] \\ \dot{S_{Y_L}} = k_{11}\dot{e_{Y_L}} + k_{92}\gamma_{Y_L} e_{Y_L}^{\gamma_{Y_L}-1}\dot{e}_{Y_L} + k_{12}[U_{YL} \\ \qquad - D_{YL} - \ddot{Y}_{dL}] \end{cases} \tag{41}$$

From (41), the virtual controllers U_{XL} and U_{YL} are expressed as follows:

$$\begin{aligned} U_{XL} &= [\ddot{X}_{dL} - \frac{k_9}{k_{10}}e\dot{X}_L - \frac{k_{91}}{k_{10}}\gamma_{X_L}e_{X_L}^{\gamma_{X_L}-1}\dot{e}_{X_L} \\ &\quad - \frac{k_{d9}}{k_{10}}|S_{X_L}|^{0.5}sgn(S_{X_L}) - \frac{k_{d10}}{k_{10}}\int sgn(S_{X_L})] \\ U_{YL} &= [\ddot{Y}_{dL} - \frac{k_{11}}{k_{12}}e\dot{Y}_L - \frac{k_{92}}{k_{12}}\gamma_{Y_L}e_{Y_L}^{\gamma_{Y_L}-1}\dot{e}_{Y_L} \\ &\quad - \frac{k_{d11}}{k_{12}}|S_{Y_L}|^{0.5}sgn(S_{Y_L}) - \frac{k_{d12}}{k_{12}}\int sgn(S_{Y_L})] \end{aligned} \quad (42)$$

The stability proof is derived based on the same concepts presented for Z loop. The robust terms of (42) are modified as follows: $U_{XLsw} = \frac{-k_{d9}}{k_{10}}|S_{X_L}|^{0.5}sgn(S_{X_L}) + v_{X_L}$; where the term v_{X_L} is calculated from the following expression: $\dot{v}_{X_L} = -\frac{k_{d10}}{k_{10}}sgn(S_{X_L})$ and $U_{YLsw} = \frac{-k_{d11}}{k_{12}}|S_{Y_L}|^{0.5}sgn(S_{Y_L}) + v_{Y_L}$; The term v_{Y_L} is calculated from the following expression: $\dot{v}_{Y_L} = -\frac{k_{d11}}{k_{12}}sgn(S_{Y_L})$. By combining the above terms with (41) and (42), $\dot{S}_{XL}$ and $\dot{S}_{YL}$ are expressed as follows:

$$\begin{aligned} \dot{S_{X_L}} &= \frac{-k_{d9}}{k_{10}}|S_{X_L}|^{0.5}sgn(S_{X_L}) + v_{X_L} - D_{XL} \\ \dot{v}_{X_L} &= -\frac{k_{d10}}{k_{10}}sgn(S_{X_L}) \\ \dot{S_{YL}} &= \frac{-k_{d11}}{k_{12}}|S_{Y_L}|^{0.5}sgn(S_{Y_L}) + v_{Y_L} - D_{YL} \\ \dot{v}_{Y_L} &= -\frac{k_{d12}}{k_{12}}sgn(S_{Y_L}) \end{aligned} \quad (43)$$

Let the Lyapunov function for X loop dynamics is chosen as follows: $V_{X_L} = 2\tau_{10}|S_{X_L}| + 0.5v_{X_L}^2 + 0.5(\tau_9|S_{X_L}|^{0.5}sgn(S_{X_L}) - v_{X_L})^2$, where as, for Y loop dynamics, the Lyapunov function is given as follows: $V_{Y_L} = 2\tau_{12}|S_{Y_L}| + 0.5v_{Y_L}^2 + 0.5(\tau_{11}|S_{Y_L}|^{0.5}sgn(S_{Y_L}) - v_{Y_L})^2$. Where $\tau_9 = \frac{k_{d9}}{k_{10}}$, $\tau_{10} = \frac{k_{d10}}{k_{10}}$,$\tau_{11} = \frac{k_{d11}}{k_{12}}$, $\tau_{12} = \frac{k_{d12}}{k_{12}}$. The following new state vectors are defined: $\eta_{XL}^T = [|S_{X_L}|^{0.5}sgn(S_{X_L})\ v_{X_L}]$; $\eta_{YL}^T = [|S_{Y_L}|^{0.5}sgn(S_{Y_L})\ v_{Y_L}]$. Define new matrices as follows: $P_{XL} = \begin{bmatrix} 4\tau_{10} + \tau_9^2 & -\tau_9 \\ -\tau_9 & 2 \end{bmatrix}$; $P_{YL} = \begin{bmatrix} 4\tau_{12} + \tau_{11}^2 & -\tau_{11} \\ -\tau_{11} & 2 \end{bmatrix}$ and then the Lyapunov functions are expressed as follows:$V_{X_L} = \zeta_1\eta_{XL}^T P_{XL}\eta_{XL} + D_{XL}^T D_{XL}$; $V_{Y_L} = \zeta_2\eta_{YL}^T P_{YL}\eta_{YL} + D_{YL}^T D_{YL}$. The time derivative of the Lyapunov functions along (43) yields the following relation:

$$\begin{aligned} \dot{V_{X_L}} &= -\zeta_1\frac{1}{\left|S_{X_L}^{0.5}\right|}\eta_{XL}^T Q_{XL}\eta_{XL} + \zeta_1 D_{XL}q_{XL}^T\eta_{XL} \\ &\quad + D_{XL}^T\dot{D}_{XL} \\ \dot{V_{Y_L}} &= -\zeta_2\frac{1}{\left|S_{Y_L}^{0.5}\right|}\eta_{YL}^T Q_{YL}\eta_{YL} + \zeta_2 D_{YL}q_{YL}^T\eta_{YL} \\ &\quad + D_{YL}^T\dot{D}_{YL} \end{aligned} \quad (44)$$

where:

$$Q_{XL} = \frac{\tau_9}{2}\begin{pmatrix} 2\tau_{10} + \tau_9^2 & -\tau_9 \\ -\tau_9 & 1 \end{pmatrix};$$

$$Q_{YL} = \frac{\tau_{11}}{2}\begin{pmatrix} 2\tau_{12} + \tau_{11}^2 & -\tau_{11} \\ -\tau_{11} & 1 \end{pmatrix}$$

and $q_{XL}^T = \left(2\tau_{10} + \frac{1}{2}\tau_9^2\ -\frac{1}{2}\tau_9\right)$;
$q_{YL}^T = \left(2\tau_{12} + \frac{1}{2}\tau_{11}^2\ -\frac{1}{2}\tau_{11}\right)$. From (44), since D_{XL} and D_{YL} are scalar quantities so $D_{XL}^T = D_{XL}$ and $D_{YL}^T = D_{YL}$, then adaptive laws are derived as follows:

$$\begin{aligned} \dot{D_{XL}} &= -\zeta_1 q_{XL}^T\eta_{XL} \\ \dot{D_{YL}} &= -\zeta_2 q_{YL}^T\eta_{YL} \end{aligned} \quad (45)$$

Applying the uncertainty bounds given in Assumption 4, and by combining (44) with (45), the simplified expressions of (44) are given as follows:

$$\begin{bmatrix} \dot{V_{XL}} = -\frac{\tau_9}{2|S_{XL}^{0.5}|}\eta_{XL}^T\tilde{Q}_{XL}\eta_{XL} \\ \dot{V_{YL}} = -\frac{\tau_{11}}{2|S_{YL}^{0.5}|}\eta_{YL}^T\tilde{Q}_{YL}\eta_{YL} \end{bmatrix} \quad (46)$$

Here, the matrices are defined as follows:

$$\tilde{Q_{XL}} = \begin{pmatrix} 2\tau_{10} + \tau_9^2 - \left(\frac{4\tau_{10}}{\tau_9} + \tau_9\right)E\Delta_{1L} & -\tau_9 + 2E\Delta_{1L} \\ -\tau_9 + 2E\Delta_{1L} & 1 \end{pmatrix}$$

and

$$\tilde{Q_{YL}} = \begin{pmatrix} 2\tau_{12} + \tau_{11}^2 - \left(\frac{4\tau_{12}}{\tau_{11}} + \tau_{11}\right)E\Delta_{2L} & -\tau_{11} + 2E\Delta_{2L} \\ -\tau_{11} + 2E\Delta_{2L} & 1 \end{pmatrix}$$

The expressions $\dot{V_{XL}}$ and $\dot{V_{YL}}$ are negative definite only if $\tilde{Q_{XL}} > 0$ and $\tilde{Q_{yL}} > 0$. If the gains satisfy the following criteria $\tau_9 > 2\ E\Delta_{1L}$, $\tau_{10} > \tau_9\frac{5\ E\Delta_{1L}\tau_9 + 4\ E\Delta_{1L}^2}{2(\tau_9 - 2\ E\Delta_{1L})}$; $\tau_{11} > 2\ E\Delta_{2L}$, $\tau_{12} > \tau_{11}\frac{5\ E\Delta_{2L}\tau_{11} + 4\ E\Delta_{2L}^2}{2(\tau_{11} - 2\ E\Delta_{2L})}$, then $\tilde{Q_{XL}} > 0$; $\tilde{Q_{YL}} > 0$ and $\dot{V}_{X_L} < 0$; $\dot{V}_{Y_L} < 0$. Here the terms $E\Delta_{1L} = D_{XL_{estimated}} - D_{XL}$; $E\Delta_{2L} = D_{YL_{estimated}} - D_{YL}$ represent estimation error of the adaptive loops.

Remark 1: Discontinuous projection operator is used to implement the adaptive laws $\dot{D_{XL}}$, $\dot{D_{YL}}$. The projection operator is defined as follows:

$$\begin{aligned} &proj D_{(X,Y)L}(\star) \\ &= \begin{cases} 0 & if\ D_{(X,Y)L} = D_{(X,Y)L_{max}};\ \star > 0 \\ 0 & if\ D_{(X,Y)L} = D_{(X,Y)L_{min}};\ \star < 0 \\ \star & otherwise \end{cases} \end{aligned} \quad (47)$$

In (45), ζ_1 and ζ_2 represent the adaptation gains. To generate reference trajectories for θ_{dL} and ϕ_{dL}, the virtual controllers U_{XL} and U_{YL} are expressed as follows:

$$\frac{U_{XL}m_{QL}}{U_{1L}} = \cos\psi_L\sin\theta_L\cos\phi_L + \sin\phi_L\sin\psi_L \quad (48)$$

$$\frac{U_{YL}m_{QL}}{U_{1L}} = \sin\psi_L\sin\theta_L\cos\phi_L - \cos\psi_L\sin\phi_L \quad (49)$$

Multiplying (48) by $\sin\psi$ and (49) by $\cos\psi$ and then taking difference of the resultant equations yields the following expression:

$$\frac{U_{XL}m_{QL}}{U_{1L}}\sin\psi - \frac{U_{YL}m_{QL}}{U_{1L}}\cos\psi = \sin\phi_{dL} \quad (50)$$

Equation (50) is simplified to get the reference command for ϕ loop of the leader UAV as follows:

$$\phi_{dL} = \sin^{-1}[\frac{U_{XL}m_{QL}}{U_{1L}}\sin\psi - \frac{U_{YL}m_{QL}}{U_{1L}}\cos\psi] \quad (51)$$

Multiplying (48) by $\cos\psi$ and (49) by $\sin\psi$ and taking the summation of the resultant equations yields the following expression:

$$\frac{U_{XL}m_{QL}}{U_{1L}}\cos\psi + \frac{U_{YL}m_{QL}}{U_{1L}}\sin\psi = \sin\theta_{dL}\cos\phi_L \quad (52)$$

Squaring (50) on both hand sides and equating $\sin^2\phi_L = 1-\cos^2\phi_L$, the expression is written in terms of $\cos\phi_L$ and given as follows:

$$\cos\phi_{dL} = \sqrt{1-[\frac{U_{XL}m_{QL}}{U_{1L}}\sin\psi - \frac{U_{YL}m_{QL}}{U_{1L}}\cos\psi]^2} \quad (53)$$

Now from (51) and (52), the reference command for θ_{dL} is expressed as follows:

$$\theta_{dL} = \sin^{-1}[\frac{\frac{U_{XL}m_{QL}}{U_{1L}}\cos\psi + \frac{U_{YL}m_{QL}}{U_{1L}}\sin\psi}{\sqrt{1-[\frac{U_{XL}m_{QL}}{U_{1L}}\sin\psi - \frac{U_{YL}m_{QL}}{U_{1L}}\cos\psi]^2}}] \quad (54)$$

B. LEADER FOLLOWERS FORMATION CONTROL

Before discussing the trajectory controllers for the follower UAVs, it is necessary to derive the formation controller which will generate the desired trajectory for the follower UAVs. Let the following sliding surface is defined for the formation controller:

$$S_{\chi_j} = \chi_j + \tau_1\int \chi_j + \tau_2\chi_j^{\gamma_{\chi_j}} \quad (55)$$

where τ_1 and τ_2 represent gain matrix of the sliding surface. By taking time derivative of (55) and combining it with (14), one obtains the following expression:

$$\dot{S_{\chi_j}} = F(\chi_j) + G(\chi_j)vj + \tau_1\chi_j + \tau_2\gamma_{\chi_j}\chi_j^{\gamma_{\chi_j}-1}\dot{\chi}_j \quad (56)$$

For the formation control, the desired longitudinal and lateral velocities of the follower UAVs are calculated as:

$$vj_{eq} = G(\chi_j)^{-1}[-F(\chi_j) - \tau_1\chi_j - \tau_2\gamma_{\chi_j}\chi_j^{\gamma_{\chi_j}-1}\dot{\chi}_j] \quad (57)$$

$$vj_{sw} = -\eta_1|S_{\chi_j}|^{0.5}sgn(S_{\chi_j}) - \eta_2\int sgn(S_{\chi_j}) \quad (58)$$

For stability proof, same procedures as adopted for *XYZ* loops, are applied here.

C. FOLLOWER UAVs CONTROL FORMULATION

In this section, we briefly explain the trajectory control of follower UAVs. As mentioned above, the reference position trajectories are generated using (18), and governed by the formation controller of (57-58). Thus, by defining the attitude, altitude and position errors for the follower UAVs, the rest of the analysis used for the derivation of the subject controllers is the same as that of the leader UAV. For simplicity, here the final control laws are included: let the attitude sliding manifolds are defined as follows:

$$\begin{aligned} S_{\phi_j} &= k_{1j}e_{\phi_j} + k_{2j}\dot{e}_{\phi_j} + k_{21j}e_{\phi_j}^{\gamma_{\phi_j}} \\ S_{\theta_j} &= k_{3j}e_{\theta_j} + k_{4j}\dot{e}_{\theta_j} + k_{34j}e_{\theta_j}^{\gamma_{\theta_j}} \\ S_{\psi_j} &= k_{5j}e_{\psi_j} + k_{6j}\dot{e}_{\psi_j} + k_{56j}e_{\psi_j}^{\gamma_{\psi_j}} \end{aligned} \quad (59)$$

where $j = [F_1, F_2]$ and F_1 and F_2 represent follower 1 and follower 2 UAVs respectively. Also k_{1j},k_{2j},k_{3j},k_{4j},k_{5j},k_{6j} represent the constants of sliding surfaces for follower UAVs. The respective errors are defined as follows: $e_{\phi_j} = \phi_j - \phi_{dj}$; $e_{\theta_j} = \theta_j - \theta_{dj}$; $e_{\psi_j} = \psi_j - \psi_{dj}$. Similarly, position and altitude sliding manifolds for follower 1 and 2 are given as:

$$\begin{aligned} S_{Zj} &= k_{7j}e_{Zj} + k_{8j}\dot{e_{Zj}} + k_{78j}e_{Z_j}^{\gamma_{Z_j}} \\ S_{Xj} &= k_{9j}e_{Xj} + k_{10j}\dot{e_{Xj}} + k_{91j}e_{X_j}^{\gamma_{X_j}} \\ S_{Yj} &= k_{11j}e_{Yj} + k_{12j}\dot{e_{Yj}} + k_{92j}e_{Y_j}^{\gamma_{Y_j}} \end{aligned} \quad (60)$$

where k_{7j}, k_{8j}, k_{9j}, k_{10j}, k_{11j}, k_{12j}, k_{78j}, k_{91j}, k_{92j} represent the constants of sliding surfaces for follower UAVs. The respective errors are defined as follows: $e_{Z_j} = Z_j - Z_{dj}$; $e_{X_j} = X_j - X_{dj}$; $e_{Y_j} = Y_j - Y_{dj}$. Now, following the same procedures, the attitude, altitude and position controllers for follower UAVs are formulated as follows:

$$\begin{aligned} U_{2jeq} = \frac{1}{b_{1j}}\Big(&\frac{-k_{1j}}{k_{2j}}\dot{e_{\phi_j}} - \frac{k_{21j}}{k_{2j}}\gamma_{\phi_j}e_{\phi_j}^{\gamma_{\phi_j}-1}\dot{e}_{\phi_j} \\ &- a_{1j}\dot{\theta_j}\dot{\psi_j} + a_{2j}\dot{\theta_j}\Omega_{rj} + \ddot{\phi}_{dj}\Big) \end{aligned} \quad (61)$$

$$U_{2jsw} = \frac{-k_{d1j}}{b_{1j}}|S_{\phi_j}|^{0.5}sgn(S_{\phi_j}) - \frac{k_{d2j}}{b_{1j}}\int sgn(S_{\phi_j}) \quad (62)$$

$$\begin{aligned} U_{3jeq} = \frac{1}{b_{2j}}\Big(&\frac{-k_{3j}}{k_{4j}}\dot{e_{\theta_j}} - \frac{k_{34j}}{k_{4j}}\gamma_{\theta_j}e_{\theta_j}^{\gamma_{\theta_j}-1}\dot{e}_{\theta_j} \\ &- a_{3j}\dot{\phi_j}\dot{\psi_j} + a_{4j}\dot{\phi_j}\Omega_{rj} + \ddot{\theta}_{dj}\Big) \end{aligned} \quad (63)$$

$$U_{3jsw} = \frac{-k_{d3j}}{b_{2j}}|S_{\theta_j}|^{0.5}sgn(S_{\theta_j}) - \frac{k_{d4j}}{b_{2j}}\int sgn(S_{\theta_j}) \quad (64)$$

$$\begin{aligned} U_{4jeq} = \frac{1}{b_{3j}}\Big(&\frac{-k_{5j}}{k_{6j}}\dot{e_{\psi_j}} - \frac{k_{56j}}{k_{6j}}\gamma_{\psi_j}e_{\psi_j}^{\gamma_{\psi_j}-1}\dot{e}_{\psi_j} - a_{5j}\dot{\phi_j}\dot{\theta_j} \\ &+ \ddot{\psi}_{dj}\Big) \end{aligned} \quad (65)$$

$$U_{4jsw} = \frac{-k_{d5j}}{b_{3j}}|S_{\psi_j}|^{0.5}sgn(S_{\psi_j}) - \frac{k_{d6j}}{b_{3j}}\int sgn(S_{\psi_j}) \quad (66)$$

$$\begin{aligned} U_{1j} = \frac{m_{Qj}}{\cos\theta_j\cos\phi_j}\Big[&g - (-\frac{k_{7}j}{k_{8j}}\dot{e_{Z_j}} - \frac{k_{78j}}{k_{8j}}\gamma_{Z_j}e_{Z_j}^{\gamma_{Z_j}-1}\dot{e}_{Z_j} \\ &+ \ddot{Z}_{dj} - \frac{k_{d7j}}{k_{8j}}|S_{Z_j}|^{0.5}sgn(S_{Z_j}) \\ &- \frac{k_{d8j}}{k_{8j}}\int sgn(S_{Z_j}))\Big] \end{aligned} \quad (67)$$

$$\begin{aligned} U_{Xj} = \ddot{X}_{dj} - \frac{k_{9j}}{k_{10j}}\dot{e_{X_j}} - \frac{k_{91j}}{k_{10j}}\gamma_{X_j}e_{X_j}^{\gamma_{X_j}-1}\dot{e}_{X_j} \\ - \frac{k_{d9j}}{k_{10j}}|S_{X_j}|^{0.5}sgn(S_{X_j}) - \frac{k_{d10j}}{k_{10j}}\int sgn(S_{X_j}) \end{aligned}$$

$$U_{Yj} = \ddot{Y}_{dj} - \frac{k_{11j}}{k_{12j}}\dot{e_{Y_j}} - \frac{k_{92j}}{k_{12j}}\gamma_{Y_j}e_{Y_j}^{\gamma_{Y_j}-1}\dot{e}_{Y_j}$$

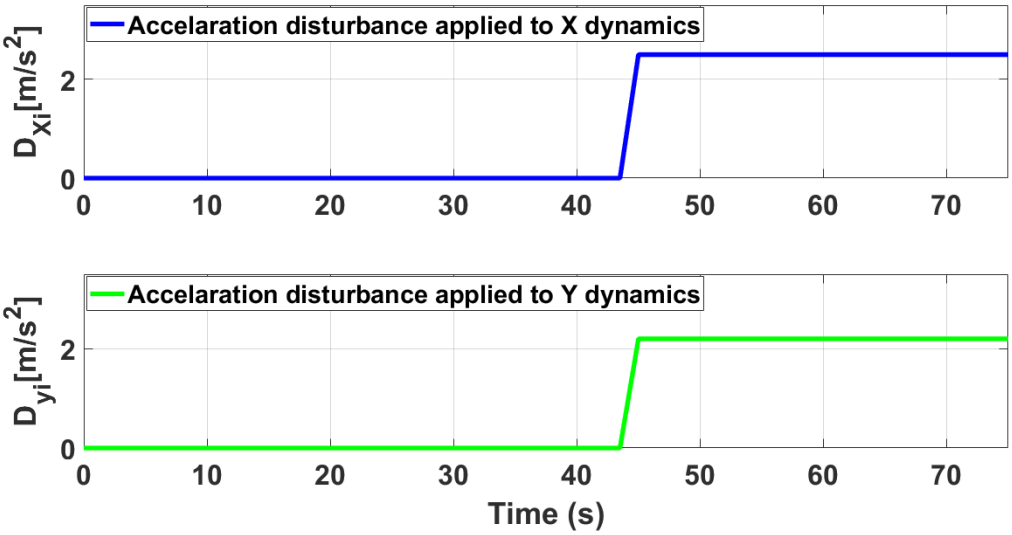

FIGURE 3. Applied acceleration type disturbance in *X* and *Y* dynamics.

$$-\frac{k_{d11j}}{k_{12j}}|S_{Y_j}|^{0.5}sgn(S_{Y_j})-\frac{k_{d12j}}{k_{12j}}\int sgn(S_{Y_j}) \quad (68)$$

$$\dot{D_{Xj}} = -\zeta_1 j S_{X_j}$$
$$\dot{D_{Yj}} = -\zeta_2 j S_{Y_j} \quad (69)$$

The reference commands for θ_{dj} and ϕ_{dj} are derived using the same procedures given in (48-54).

D. FOLLOWER GROUND ROBOT TRAJECTORY CONTROL

In this subsection, the trajectory control of ground robot is discussed based on the idea presented in [50]. The reference trajectory of the ground robot is generated using (18), (57) and (58). The kinematic model of the ground robot is expressed as follows:

$$\begin{bmatrix}\dot{x}_{robot}\\ \dot{y}_{robot}\\ \dot{\vartheta}\end{bmatrix}=\begin{bmatrix}\cos\vartheta & -a\sin\vartheta\\ \sin\vartheta & a\cos\vartheta\\ 0 & 1\end{bmatrix}\begin{bmatrix}u\\ \omega\end{bmatrix}+\begin{bmatrix}D_{x_{robot}}\\ D_{y_{robot}}\\ 0\end{bmatrix} \quad (70)$$

Similarly, the dynamic equations of the ground robot are represented as follows:

$$\begin{bmatrix}\dot{u}\\ \dot{\omega}\end{bmatrix}=\begin{bmatrix}\frac{\theta_3}{\theta_1}\omega^2-\frac{\theta_4}{\theta_1}u\\ -\frac{\theta_5}{\theta_2}u\omega-\frac{\theta_6}{\theta_2}\omega\end{bmatrix}+\begin{bmatrix}\frac{1}{\theta_1} & 0\\ 0 & \frac{1}{\theta_2}\end{bmatrix}\begin{bmatrix}u_r\\ \omega_r\end{bmatrix}+\begin{bmatrix}D_u\\ D_\omega\end{bmatrix} \quad (71)$$

Here u and w represent the linear and angular velocities respectively, x_{robot}, y_{robot} denote the position of robot in inertial frame, ϑ represents robot orientation,$D_{xrobot}, D_{yrobot}, D_u, D_w$ are the uncertainty terms in dynamics and kinematics of the robot respectively. Moreover the parameters θ_i with $i = 1, 2, 3, 4, 5, 6$ are expressed as follows [50]:

$$\theta_1 = \left[\frac{R_a}{k_a}\left(m_r r^2+2I_e\right)+2rk_{DT}\right]\frac{1}{(2rk_{PT})}$$
$$\theta_2 = \left[\frac{R_a}{k_a}\left(I_e d^2+2r^2\left(I_{zr}+m_r b^2\right)\right)+2rdk_{DR}\right]\frac{1}{(2rdk_{PR})}$$
$$\theta_3 = \frac{R_a}{k_a}\frac{m_r br}{2k_{PT}}$$
$$\theta_4 = \frac{R_a}{k_a}\left(\frac{k_a k_b}{R_a}+B_e\right)\frac{1}{rk_{PT}}+1$$
$$\theta_5 = \frac{R_a}{k_a}\frac{m_r br}{dk_{PR}}$$
$$\theta_6 = \frac{R_a}{k_a}\left(\frac{k_a k_b}{R_a}+B_e\right)\frac{d}{2rk_{PR}}+1$$

In the above expressions, m_r represents mass of the robot, I_{zr} is its moment of inertia at G, R_a, k_b and k_a represent resistance, back emf constant, and torque constants of motors respectively, B_e represents coefficient of friction, I_e is the moment of inertia of each group rotor-reduction gearwheel, r is the radius of each wheel. $k_{PT} > 0$ and $k_{PR} > 0, k_{DT} \geq 0$ and $k_{DR} \geq 0$ represent the control gains of motor internal loops.

The kinematic controller proposed in [52] is utilized for the outer loop. The control equations are given as follows:

$$\begin{bmatrix}u_d\\ \omega_d\end{bmatrix}=\begin{bmatrix}\cos\vartheta & \sin\vartheta\\ -\frac{1}{a}\sin\vartheta & \frac{1}{a}\cos\vartheta\end{bmatrix}\times\begin{bmatrix}\dot{x}_{d-robot}+l_x\tanh\left(\frac{k_x}{l_x}\tilde{x}_{robot}\right)\\ \dot{y}_{d-robot}+l_y\tanh\left(\frac{k_y}{l_y}\tilde{y}_{robot}\right)\end{bmatrix} \quad (72)$$

Here $\tilde{x}_{robot}$ and $\tilde{y}_{robot}$ represent the positions error. Similarly, the dynamic model of (71) is re-organized as follows [50]:

$$\mathbf{v_r} = \mathbf{H}\dot{\mathbf{v}}' + \mathbf{C}\left(\mathbf{v}'\right)\mathbf{v}' + \mathbf{F}\left(\mathbf{v}'\right)\mathbf{v}' + \Delta \quad (73)$$

where, from (73) we have:

$$\mathbf{H} = \begin{bmatrix}\theta_1/i & 0\\ 0 & \theta_2\end{bmatrix},$$
$$\mathbf{F}\left(\mathbf{v}'\right) = \begin{bmatrix}\theta_4/i & 0\\ 0 & \theta_6+(\theta_5/i-\theta_3)iu\end{bmatrix},$$

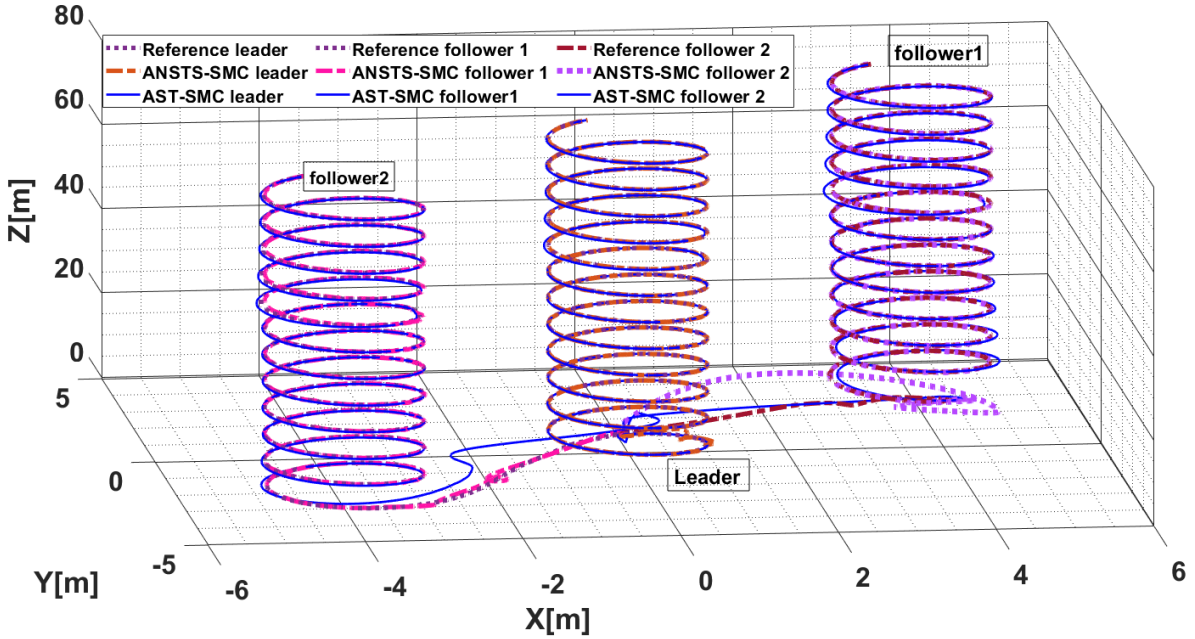

FIGURE 4. UAVs *XYZ* trajectory tracking comparison under acceleration type disturbances.

TABLE 1. Leader-followers UAV parameters.

Symbol	Value	Unit
$m_{QL} = m_{F1} = m_{F1}$	0.65	kg
$l_L = l_{F1} = l_{F2}$	0.23	m
$J_{rL} = J_{F1} = J_{F2}$	$6.5 * 10^{-5}$	$kg.m^2$
$I_{xL} = I_{xF1} = I_{xF2}$	$7.5 * 10^{-3}$	Ns^2rad^{-1}
$I_{yL} = I_{yF1} = I_{yF2}$	$7.5 * 10^{-3}$	Ns^2rad^{-1}
$I_{zL} = I_{zF1} = I_{zF2}$	$1.3 * 10^{-2}$	Ns^2rad^{-1}

$$\mathbf{C}\left(\mathbf{v}'\right) = \begin{bmatrix} 0 & -\theta_3\omega \\ \theta_3\omega & 0 \end{bmatrix},$$

$$\Delta = \begin{bmatrix} -\theta_1 & 0 \\ 0 & -\theta_2 \end{bmatrix} \begin{bmatrix} D_u \\ D_\omega \end{bmatrix},$$

$$\mathbf{v}' = \begin{bmatrix} i & 0 \\ 0 & 1 \end{bmatrix} \begin{bmatrix} u \\ \omega \end{bmatrix}.$$

So, the dynamic controller is expressed as follows:

$$\mathbf{v_r} = \mathbf{H}\left(\dot{\mathbf{v}}'_\mathbf{d} + \mathbf{T}\left(\tilde{\mathbf{v}}'\right)\right) + \mathbf{C}\mathbf{v}'_\mathbf{d} + \mathbf{F}\mathbf{v}'_\mathbf{d} \tag{74}$$

It is assumed that $\mathbf{H}$,$\mathbf{F}$ and $\mathbf{C}$ are known quantities. The modified velocities vector is expressed as follows [52]: $\mathbf{v}'_\mathrm{d} = \begin{bmatrix} u'_d \\ \omega_d \end{bmatrix} = \begin{bmatrix} i & 0 \\ 0 & 1 \end{bmatrix} \begin{bmatrix} u_d \\ \omega_d \end{bmatrix}$. Moreover the term $\mathbf{T}\left(\tilde{\mathbf{v}}'\right)$ is expressed as follows: $\mathbf{T}\left(\tilde{\mathbf{v}}'\right) = \begin{bmatrix} l_u & 0 \\ 0 & l_\omega \end{bmatrix} \begin{bmatrix} \tanh\left(\frac{k_u}{l_u} i\tilde{u}\right) \\ \tanh\left(\frac{k_\omega}{l_\omega} \tilde{\omega}\right) \end{bmatrix}$. The controller gains satisfy the following criteria: $k_u > 0, k_\omega > 0$. Moreover, $l_u \in \mathbb{R}$ and $l_\omega \in \mathbb{R}$ are saturation gains and $\tilde{\omega} = \omega_d - \omega$ and $\tilde{u} = u_d - u$ are the current velocity errors.

IV. RESULTS AND DISCUSSION

In this section, the proposed ANSTS-SMC is tested numerically for the system of leader follower configuration shown

TABLE 2. Leader UAV control parameters for attitude, altitude and position loops.

Parameter	Value	Parameter	Value
k_1	200	k_2	1
k_{d1}	70	k_{d2}	15
k_3	200	k_4	1
k_{d3}	50	k_{d4}	10
k_5	95	k_6	1
k_{d5}	4.6	k_{d6}	0.5
k_7	97	k_8	1
k_{d7}	300	k_{d8}	1.5
k_9	60	k_{10}	1000
k_{d9}	2.5	k_{d10}	180
k_{11}	60	k_{12}	1000
k_{d11}	2.5	k_{d12}	5
ζ_1	1.5	ζ_2	2.5
k_{21}	500	k_{34}	250
k_{56}	50	k_{78}	25
k_{91}	150	k_{92}	85
γ_{θ_L}	0.25	γ_{ϕ_L}	0.25
γ_{X_L}	0.45	γ_{Y_L}	0.45
γ_{Z_L}	0.45	γ_{ψ_L}	0.25

TABLE 3. Follower UAVs control parameters for attitude, altitude and position loops.

Parameter	Value	Parameter	Value
k_{1j}	200	k_{2j}	1
k_{d1j}	70	k_{d2j}	15
k_{3j}	200	k_{4j}	1
k_{d3j}	50	k_{d4j}	10
k_{5j}	95	k_{6j}	1
k_{d5j}	4.6	k_{d6j}	0.5
k_{7j}	97	k_{8j}	1
k_{d7j}	300	k_{d8j}	1.5
k_{9j}	60	k_{10j}	1000
k_{d9j}	2.5	k_{d10j}	180
k_{11j}	60	k_{12j}	1000
k_{d11j}	2.5	k_{d12j}	5
ζ_{1j}	1.5	ζ_{2j}	2.5
k_{21j}	500	k_{34j}	250
k_{56j}	50	k_{78j}	25
k_{91j}	150	k_{92j}	85

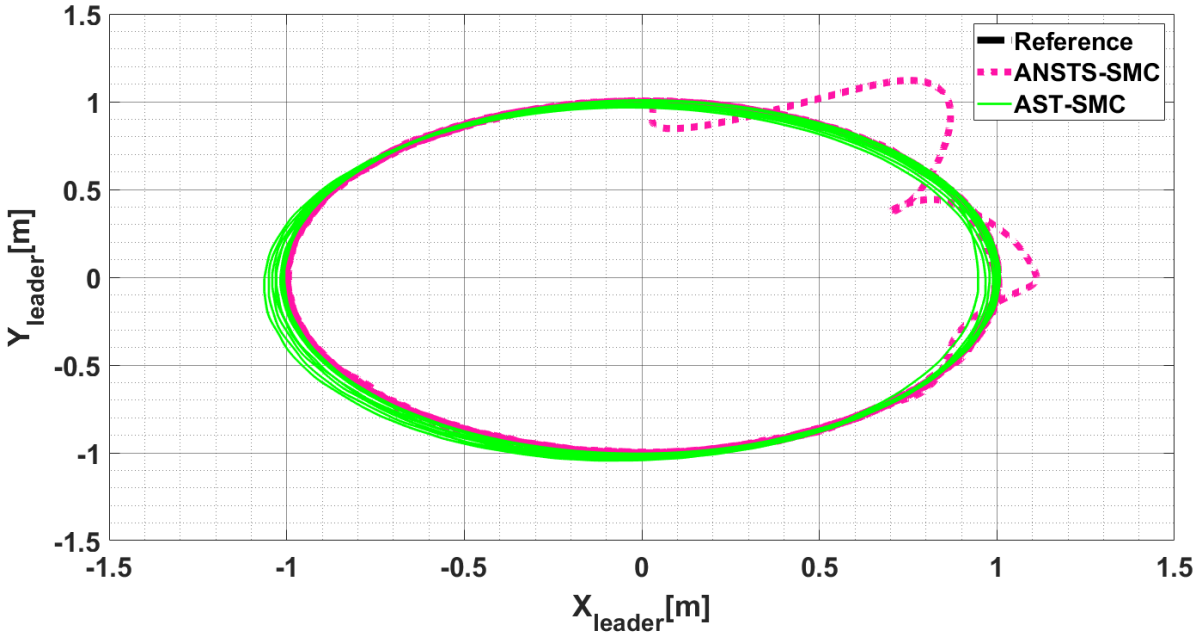

FIGURE 5. *XY* leader UAV trajectory tracking comparison under acceleration type disturbances.

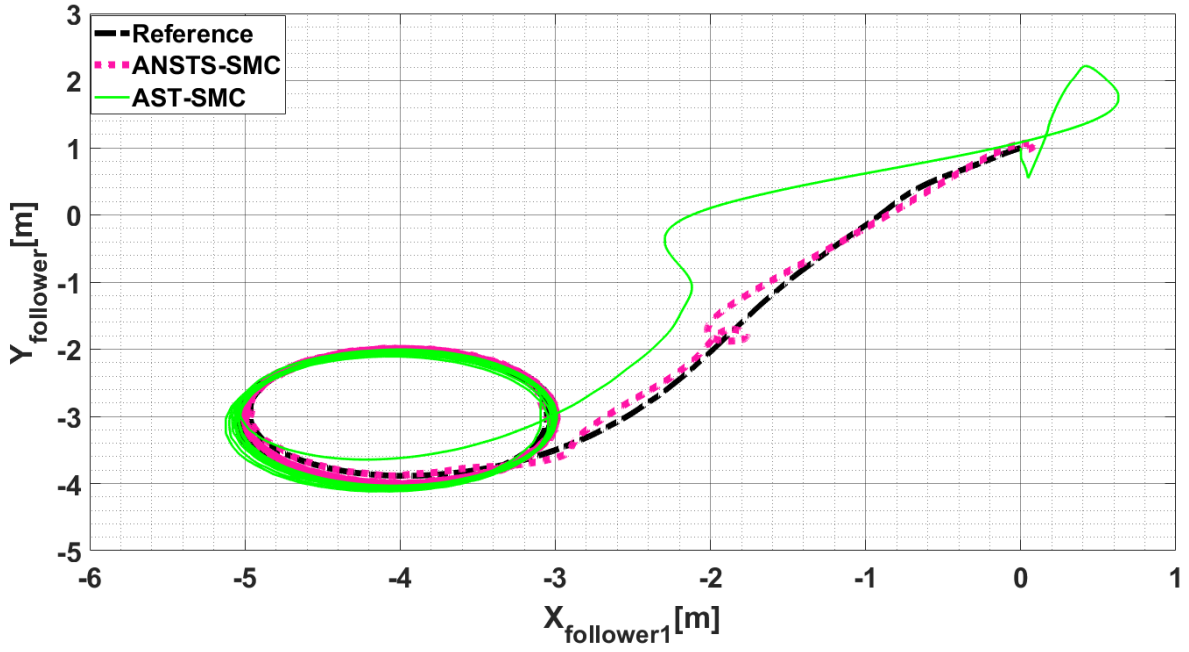

FIGURE 6. *XY* follower 1 UAV trajectory tracking comparison under acceleration type disturbances.

in Fig. 2. The parameters of the leader and followers UAVs are identical and are given in Table 1. Moreover, the parameters of UGV are given in [52]. The control parameters of leader and follower UAVs are given in Table 2 and 3, while the controller parameters of UGV are the same as given in [52]. Since the UAVs are identical, thus leader and follower UAVs use the same control parameters. The parameters for formation control loops are chosen as follows: $\tau_{F1} = \tau_{F2} = \tau_{F3} = \begin{bmatrix} 1.5 \\ 1.5 \\ 0.5 \end{bmatrix}$, $\eta_{1F1} = \eta_{1F2} = \eta_{1F3} = \begin{bmatrix} 0.1 \\ 0.1 \\ 0.075 \end{bmatrix}$, $\eta_{2F1} = \eta_{2F2} = \eta_{2F3} = \begin{bmatrix} 0.05 \\ 0.05 \\ 0.02 \end{bmatrix}$. For the leader UAV, the reference position

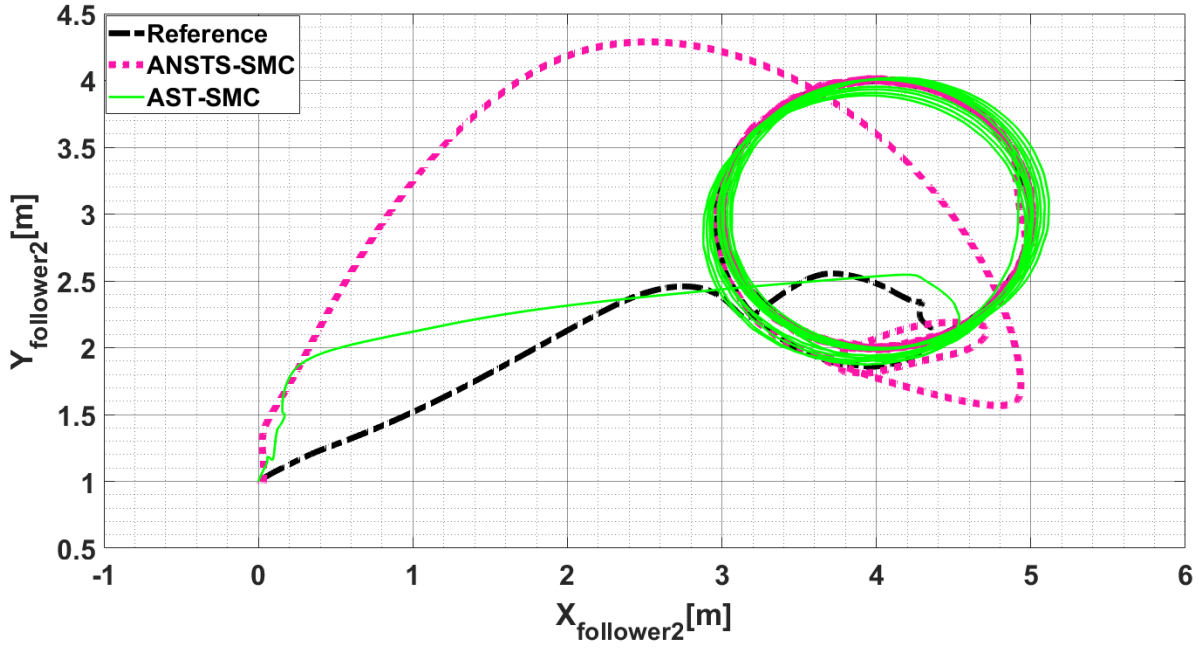

FIGURE 7. *XY* follower 2 UAV trajectory tracking comparison under acceleration type disturbances.

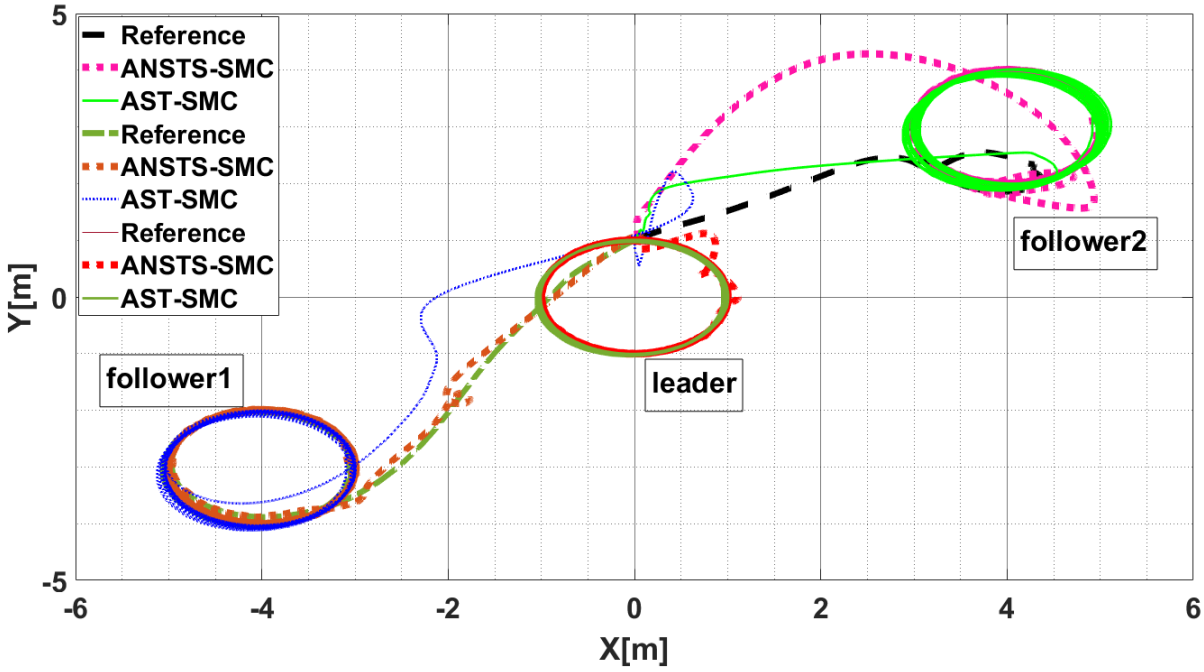

FIGURE 8. *XY* Leader-followers UAV trajectory tracking comparison under acceleration type disturbances.

and altitude commands are set as follows: $X_L = 0.1t \sin t$, $Y_L = 0.1t \cos t$ and $Z_L = t$. Figure 3 shows the applied acceleration disturbance on X and Y dynamics of the leader and follower UAVs. It is assumed that same type of disturbance acceleration is applied for all UAVs. Furthermore, the disturbance acceleration has no effect on the Z dynamics of UAV. Moreover, the following parametric uncertainties are applied: $a_{1L} = 2.5a_{1L}$; $a_{1j} = 2.5a_{1j}$; $a_{2L} = 2.5a_{2L}$; $a_{2j} = 2.5a_{2j}$; $a_{3L} = 2.5a_{3L}$; $a_{3j} = 2.5a_{3j}$; $a_{4L} = 2.5a_{4L}$; $a_{4j} = 2.5a_{4j}$; $a_{5L} = 2.5a_{5L}$; $a_{5j} = 2.5a_{5j}$; $b_{1L} = 1.75b_{1L}$; $b_{1j} = 1.75b_{1j}$; $b_{2L} = 1.75b_{2L}$;$b_{2j} = 1.75b_{2j}$; $b_{3L} = 1.75b_{3L}$; $b_{3j} = 1.75b_{3j}$.

Figure 4 shows the trajectory tracking simulations of leader follower UAVs in the presence of applied disturbance of

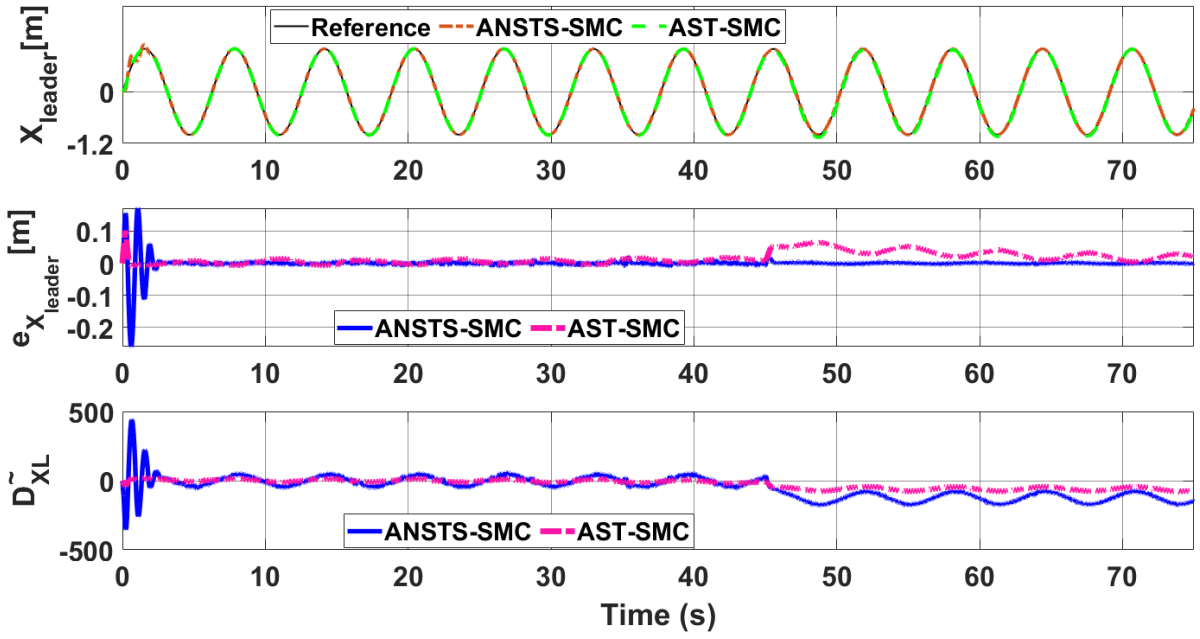

FIGURE 9. X_{leader} UAV tracking comparison under acceleration type disturbances.

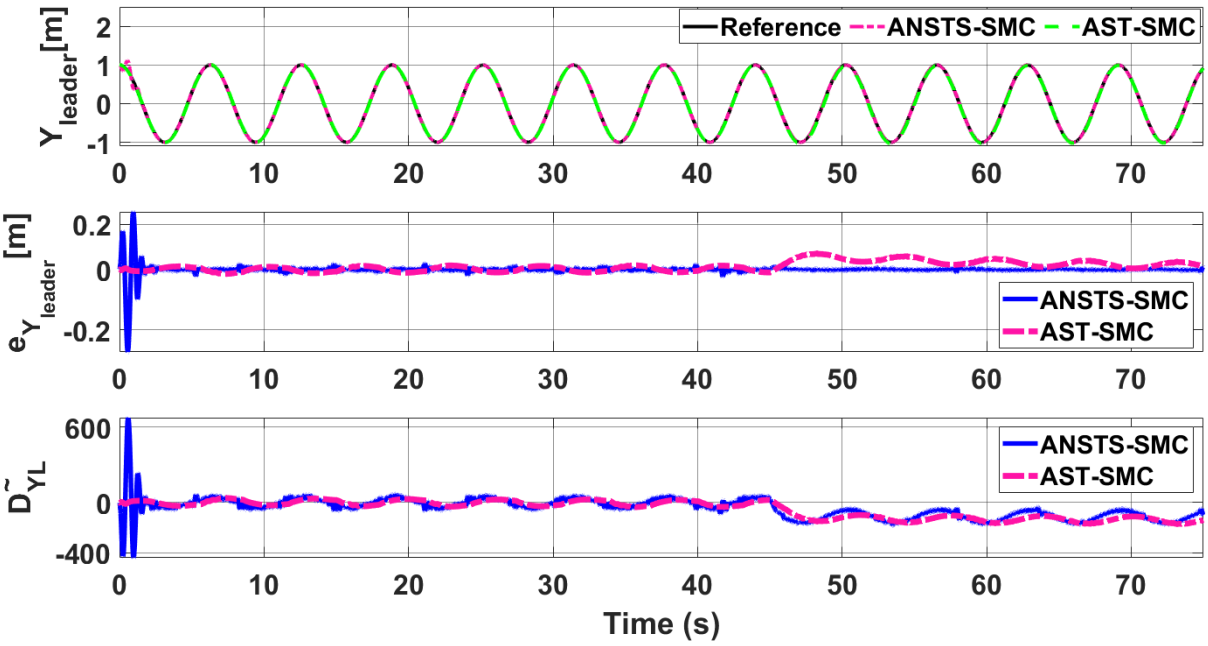

FIGURE 10. Y_{leader} UAV tracking comparison under acceleration type disturbances.

Figure 3. From the presented results, it is concluded that in the presence of disturbances, ANSTS-SMC controllers ensure robust behaviour, while AST-SMC controllers produces steady state errors while tracking responses of the leader and follower UAVs in the X and Y direction.

Table 4 shows the trajectory tracking comparison between AST-SMC and ANSTS-SMC at 45 seconds when the wind disturbances are applied to the quad-rotor. It shows the robustness of the ANSTS-SMC algorithm in terms of low error generated as compared to AST-SMC algorithm. In order to have a clear picture of the trajectory deviations under wind disturbance, Figures 5-8 show the trajectory tracking comparisons in XY plane for leader, follower 1 and follower 2 UAVs respectively. From the presented results, it is

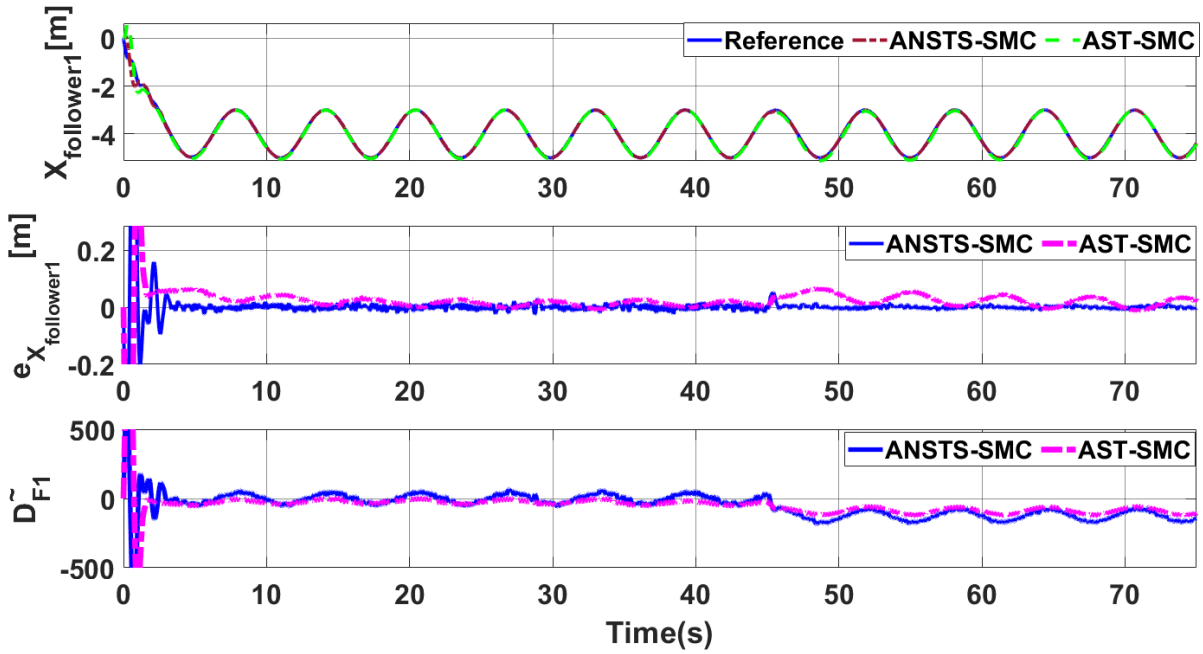

FIGURE 11. X_{F1} UAV tracking comparison under acceleration type disturbances.

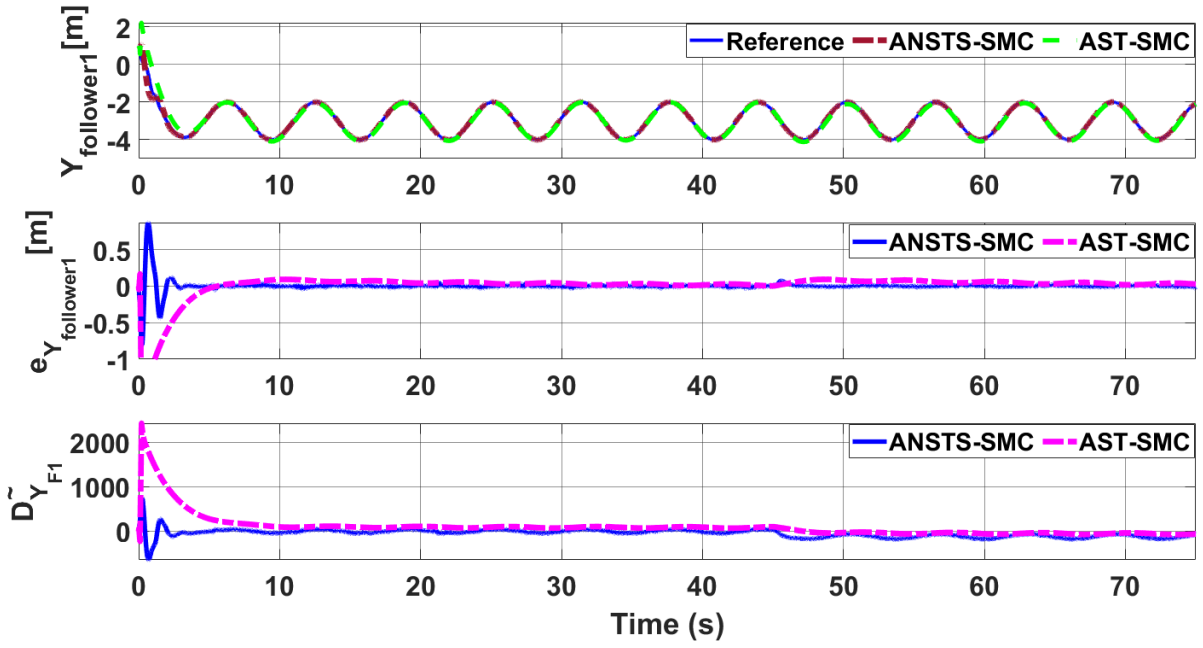

FIGURE 12. Y_{F1} UAV tracking comparison under acceleration type disturbances.

TABLE 4. Trajectory tracking comparison of ANSTS-SMC and AST-SMC algorithms at time = 45s.

Tracking Error	AST-SMC	ANSTS-SMC
e_{XL}	0.05 m	0 m
e_{YL}	0.05 m	0.01 m
$e_{X_{F1}}$	0.1 m	0.01 m
$e_{Y_{F1}}$	0.1 m	0.02 m
$e_{X_{F2}}$	0.05 m	0.01 m
$e_{Y_{F2}}$	0.1 m	0.02 m

concluded that minimum deviations are observed in the trajectory tracking for all UAVs with ANSTS-SMC controllers, while with AST-SMC controllers all UAVs show significant drift from the reference trajectories in XY plane. The trajectory tracking comparison of the controllers in X and Y plane for leader and follower quad-rotors is presented in figures 9-14. In these figures, the value of tracking error is quantified. Figure 8 shows the combined trajectories of leader follower UAVs with ANSTS-SMC and AST-SMC controllers

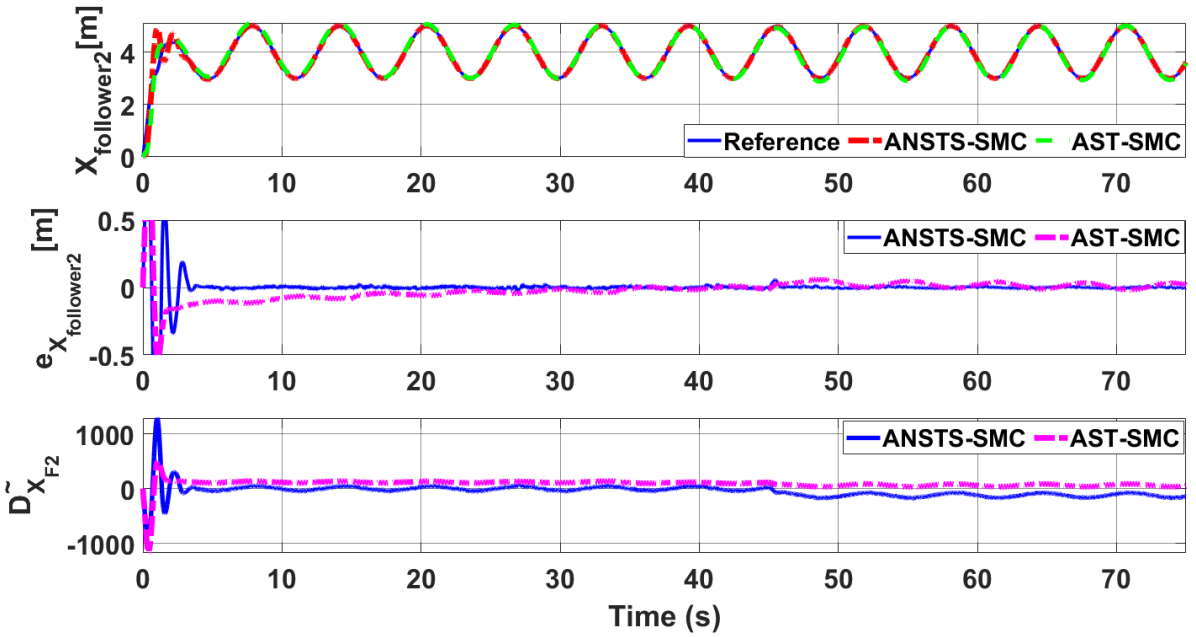

FIGURE 13. X_{F2} UAV tracking comparison under acceleration type disturbances.

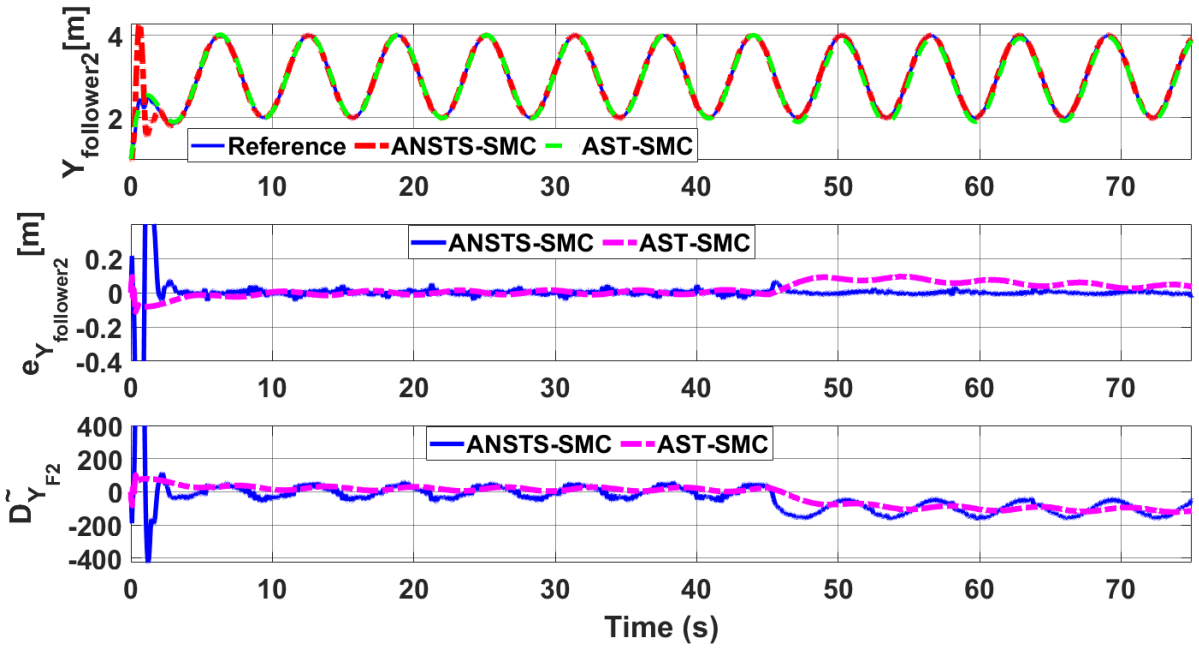

FIGURE 14. Y_{F2} UAV tracking comparison under acceleration type disturbances.

in XY plane. From the presented results, it is evident that the proposed ANSTS-SMC controllers ensure robust formation control between the leader and follower UAVs and has less tracking error, while with AST-SMC, all UAVs show drift in their trajectories.

In order to compare the trajectory tracking performance of the leader followers UAV quantitatively, the X and Y trajectories are individually plotted against time and the results are presented in figure 9 and 10 for the leader UAV. From Figure 9, and at time $t = 45sec$, the e_{XL} tracking error is 0.05 m with AST-SMC while with ANSTS-SMC, the measured error e_{XL} is approximately zero. ANSTS-SMC ensures lowest error of magnitude 0 due the adaptive disturbance compensation term D_{XL} and from the presented results of figure 9, it is obvious that at time $t = 45s$, the adaptive term D_{XL} adds appropriate compensation to cancel the

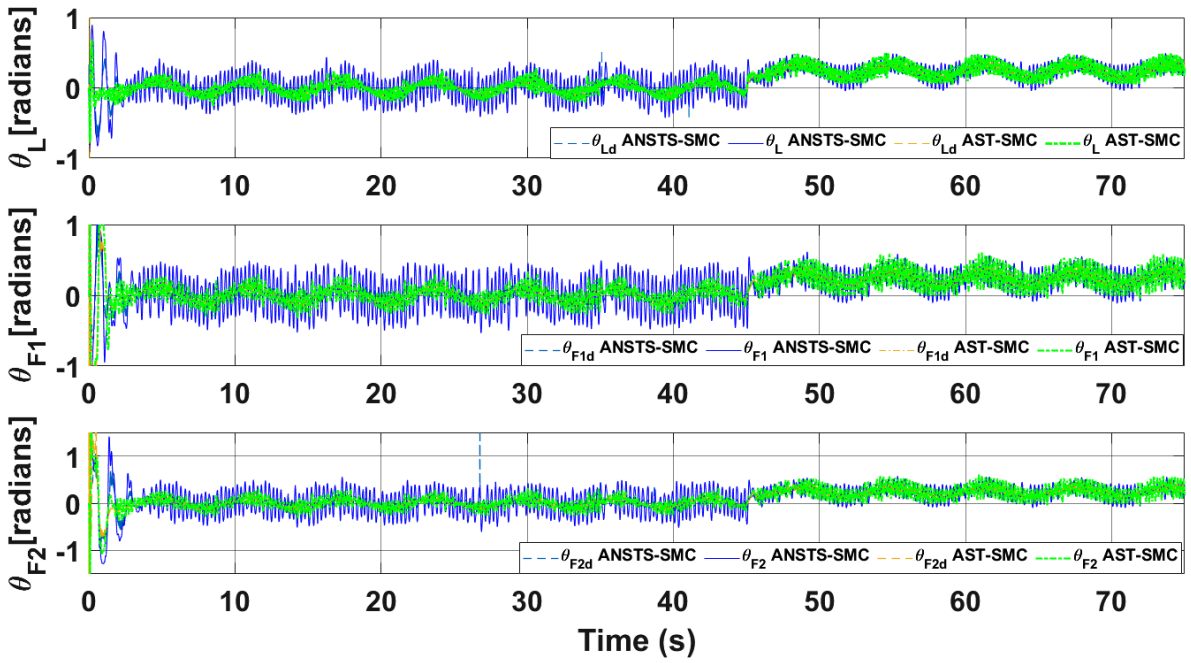

FIGURE 15. UAV θ tracking comparison under acceleration type disturbances.

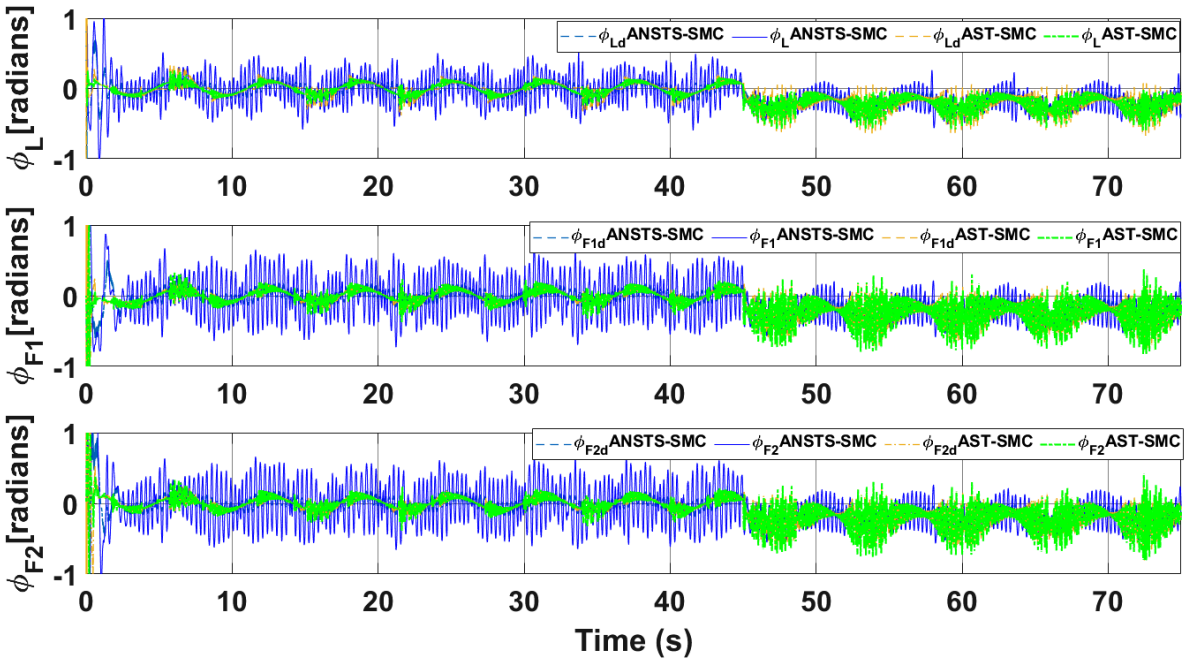

FIGURE 16. UAV ϕ tracking comparison under acceleration type disturbances.

disturbance and it switches from 50 to -200. Similarly, from figure 10, e_{YL} is measured as 0.05m and 0.01m with AST-SMC and ANSTS-SMC respectively. ANSTS-SMC offers lowest error of 0.01m due to the adaptive estimator term D_{YL}. From figure 10, it is obvious that at time $t = 45s$, the adaptive term D_{YL} adds appropriate compensation to cancel the disturbance and it switches from 0 to -200.

Similarly, for follower UAVs, the X and Y tracking responses are plotted against simulation time in figure 11-14. From the presented results and at time $t = 45s$, the measured error signals with AST-SMC are as follows: $e_{X_{F1}} = 0.1m$, $e_{Y_{F1}} = 0.1m$, $e_{X_{F2}} = 0.05m$, $e_{Y_{F2}} = 0.1m$, while with ANSTS-SMC, the errors are measured as follows: $e_{X_{F1}} = 0.01m$, $e_{Y_{F1}} = 0.02m$, $e_{X_{F2}} = 0.01m$, $e_{Y_{F2}} = 0.02m$. From the presented results of figures 11-14, it is obvious that at

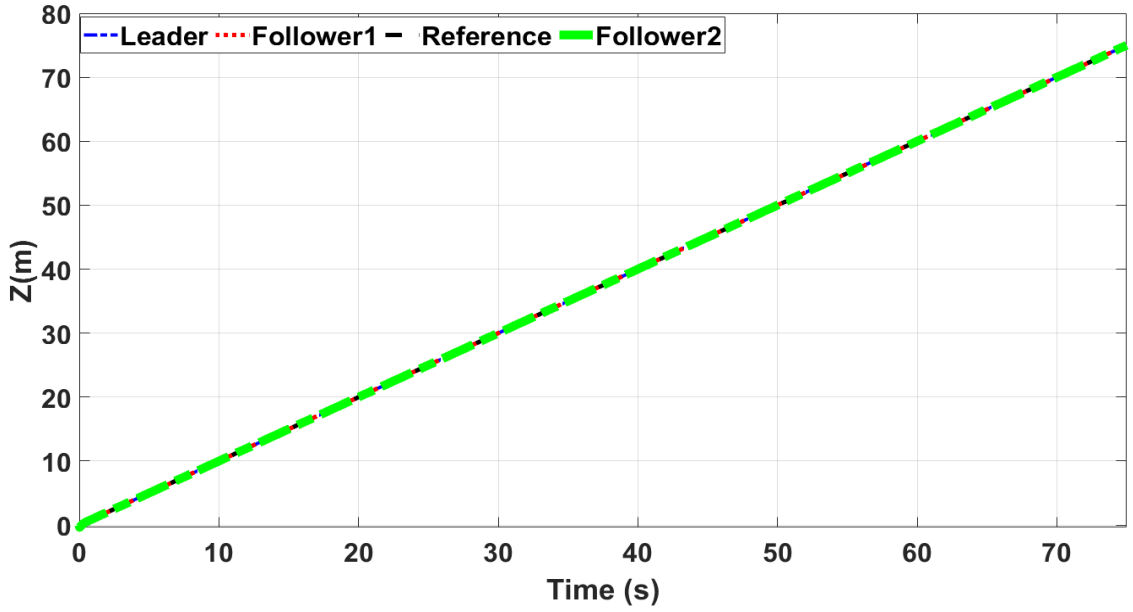

FIGURE 17. UAVs Z tracking.

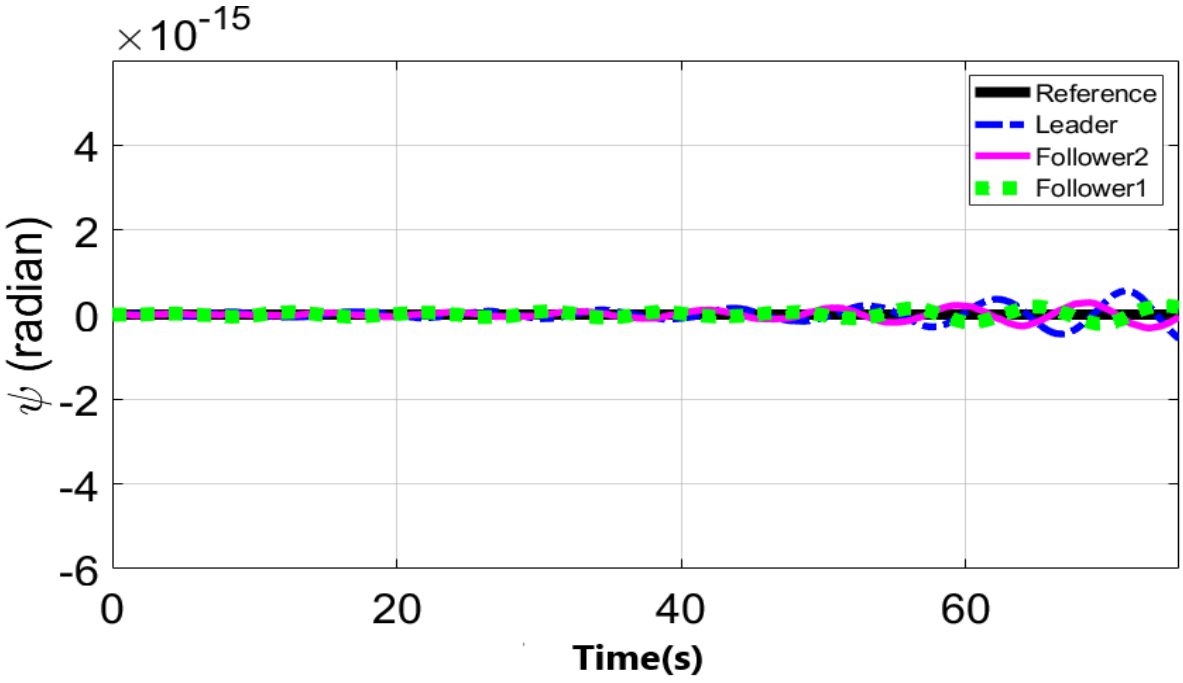

FIGURE 18. UAVs ψ tracking.

time $t = 45s$, the adaptive terms $D_{X_{F1}}$,$D_{Y_{F1}}$, $D_{X_{F2}}$,$D_{Y_{F2}}$ add appropriate compensation to cancel the disturbances.

Figure 15 and 16 show θ and ϕ tracking responses for leader and follower UAVs with both AST-SMC and ANSTS-SMC respectively. From the presented results and at time $t = 45s$, it is evident that the proposed ANSTS-SMC generate appropriate reference commands for both θ and ϕ loops of leader and follower UAVs.

Figure 17 and 18 show Z and ψ loops tracking responses for leader and follower UAVs. Since no disturbances are applied on both of these loops, thus the tracking responses under AST-SMC and ANSTS-SMC are comparable. Finally figure 19 shows the robustness of the formation controllers for tracking the respective reference commands i.e. the distance between the leader and the followers in XY plane. From the presented results, it is obvious that apart from the

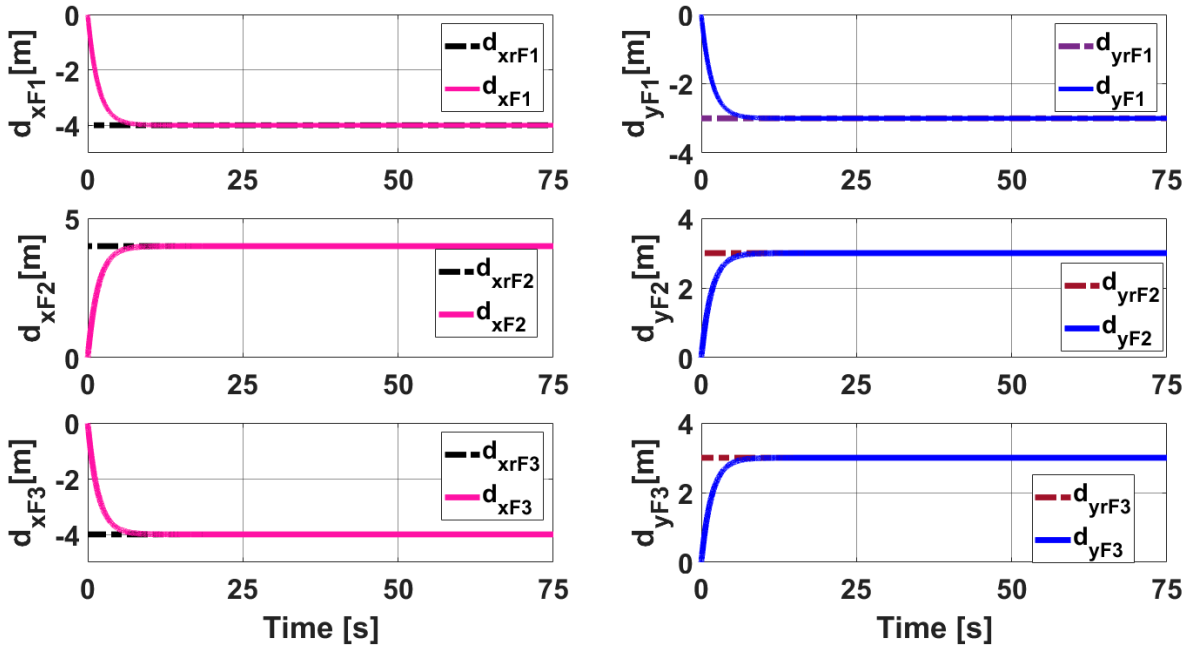

FIGURE 19. Formation controller tracking.

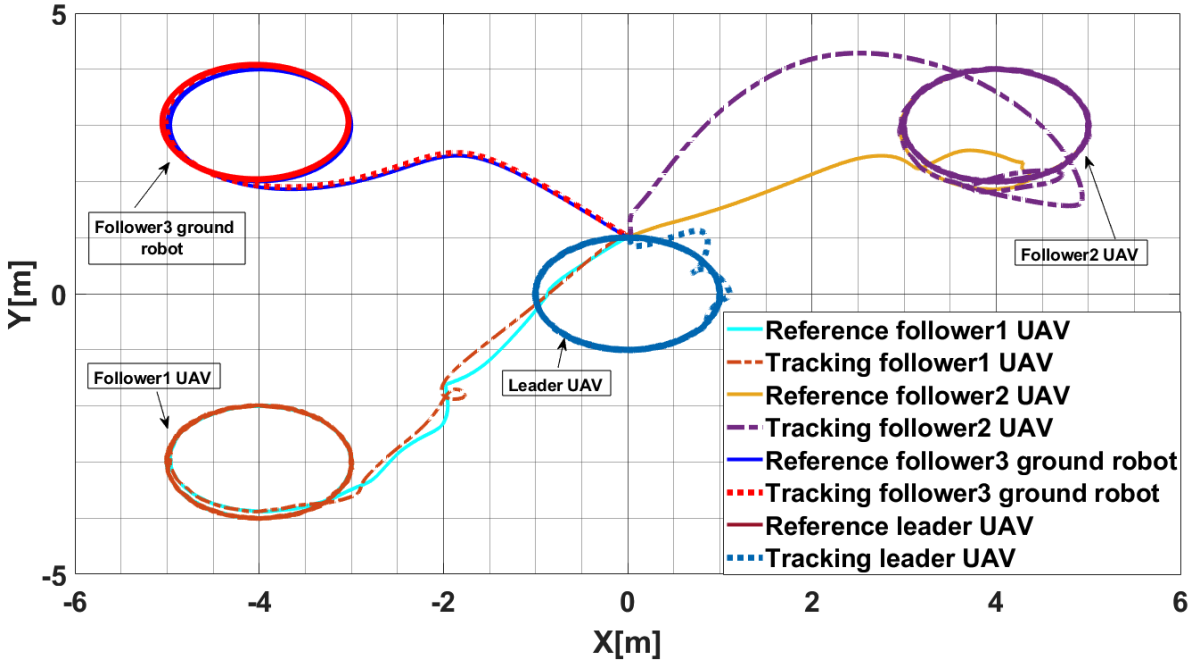

FIGURE 20. *XY* UAVs and UGV leader follower trajectory tracking comparison.

transient error, the formation controllers accurately maintain the desired distance between the leader-follower1, leader-follower2 and leader-follower3 UAV and UGV.

Figure 20 shows the simulation results of the formation between UAVs and UGV vehicle. From the presented results, it is obvious that all the followers (UAVs and UGV) accurately form the leader follower configuration and moreover each follower also follow the respective reference trajectory generated in *XY* plane.

V. CONCLUSION

This paper proposed an adaptive non-singular terminal super twisting sliding mode trajectory and formation controllers for multiple UAVs flying in the leader follower configuration.

Acceleration type disturbances and parametric uncertainties are applied to X and Y dynamics of leader and follower UAVs. The formation control of UAVs is tested with the proposed ANSTS-SMC and AST-SMC algorithms. The robust performance of the proposed controller is verified from the measured errors of the leader and follower UAVs presented in the discussion section. For leader UAV, the errors are $e_{XL} = 0\ m$, $e_{YL} = 0.01m$ with ANSTS-SMC control while with AST-SMC, the measured errors are as follows: $e_{XL} = 0.05m$, $e_{YL} = 0.05m$. Similarly for follower UAVs, the errors are $e_{X_{F1}} = 0.01m$, $e_{Y_{F1}} = 0.02m$, $e_{X_{F2}} = 0.01m$, $e_{Y_{F2}} = 0.02m$ with ANSTS-SMC algorithm while with AST-SMC, the measured errors are as follows: $e_{X_{F1}} = 0.1m$, $e_{Y_{F1}} = 0.1m$, $e_{X_{F2}} = 0.05m$, $e_{Y_{F2}} = 0.1m$. Moreover, the settling time of XY states of ANSTS-SMC after the occurrence of disturbances is upto 1 second which is faster as compared to AST-SMC control methods. The trajectory tracking comparison for a ground based unicycle mobile robot in leader follower formation with a quad-copter is also presented, however the tracking signal suffers from steady state error due to non adaptive control loops and fixed gains of unicycle robot. From the quantitative comparison, it is concluded that the proposed ANSTS-SMC algorithm show enhanced robust behaviour to the acceleration type disturbances and parametric uncertainties of the system as compared to AST-SMC algorithms.

REFERENCES

[1] H. Shakhatreh, A. H. Sawalmeh, A. Al-Fuqaha, Z. Dou, E. Almaita, I. Khalil, N. S. Othman, A. Khreishah, and M. Guizani, "Unmanned aerial vehicles (UAVs): A survey on civil applications and key research challenges," *IEEE Access*, vol. 7, pp. 48572–48634, 2019.

[2] Research and Markets. *The Global UAV Payload Market 2017–2027*. Accessed: Sep. 2020. Available:. [Online]. Available: https://www.researchandmarkets.com/research/nfpsbm/theglobalUAV

[3] N. S. Özbek and M. Ö. Efe, "Feedback control strategies for quadrotor-type aerial robots: A survey," *Trans. Inst. Meas. Control*, vol. 38, no. 5, pp. 529–554, May 2016.

[4] A. Kacimi, A. Mokhtari, and B. Kouadri, "Sliding mode control based on adaptive backstepping approch for a quadrotor unmanned aerial vehicle," *Przegląd Elektrotechniczny*, vol. 88, no. 6, pp. 188–193, Jan. 2012.

[5] X. Liu, H. Wang, D. Fu, Q. Yu, P. Guo, Z. Lei, and Y. Shang, "An area-based position and attitude estimation for unmanned aerial vehicle navigation," *Sci. China Technol. Sci.*, vol. 58, no. 5, pp. 916–926, May 2015.

[6] T. X. Dinh, D. N. C. Nam, and K. K. Ahn, "Robust attitude control and virtual reality model for quadrotor," *Int. J. Autom. Technol.*, vol. 9, no. 3, pp. 283–290, May 2015.

[7] T. Madani and A. Benallegue, "Sliding mode observer and backstepping control for a quadrotor unmanned aerial vehicles," in *Proc. Amer. Control Conf.*, Jul. 2007, pp. 5887–5892.

[8] Y. Alothman, W. Jasim, and D. Gu, "Quad-rotor lifting-transporting cable-suspended payloads control," in *Proc. 21st Int. Conf. Autom. Comput. (ICAC)*, Sep. 2015, pp. 1–6.

[9] T. Dierks and S. Jagannathan, "Output feedback control of a quadrotor UAV using neural networks," *IEEE Trans. Neural Netw.*, vol. 21, no. 1, pp. 50–66, Jan. 2010.

[10] P. J. Cruz, M. Oishi, and R. Fierro, "Lift of a cable-suspended load by a quadrotor: A hybrid system approach," in *Proc. Amer. Control Conf. (ACC)*, Jul. 2015, pp. 1887–1892.

[11] A. Ibeas, N. Ullah, M. A. Ali, and J. A. Herrera, "Control deslizante fraccionario de la trayectoria y orientación de un quadrotor con cargas suspendidas desconocidas," *Revista Iberoamericana de Automática e Informática Ind.*, vol. 16, no. 3, pp. 321–331, Nov. 2018, doi: 10.4995/riai.2018.9951.

[12] R. Abbas and Q. Wu, "Tracking formation control for multiple quadrotors based on fuzzy logic controller and least square oriented by genetic algorithm," *Open Autom. Control Syst. J.*, vol. 7, no. 1, pp. 842–850, Aug. 2015.

[13] C. Hua, J. Chen, and Y. Li, "Leader-follower finite-time formation control of multiple quadrotors with prescribed performance," *Int. J. Syst. Sci.*, vol. 48, no. 12, pp. 2499–2508, Sep. 2017.

[14] F. Wu, J. Chen, and Y. Liang, "Leader-follower formation control for quadrotors," *IOP Conf. Ser., Mater. Sci. Eng.*, vol. 187, Mar. 2017, Art. no. 012016.

[15] K. A. Ghamry and Y. Zhang, "Formation control of multiple quadrotors based on leader-follower method," in *Proc. Int. Conf. Unmanned Aircr. Syst. (ICUAS)*, Denver, CO, USA, Jun. 2015, pp. 1037–1042.

[16] B. Mu, K. Zhang, and Y. Shi, "Integral sliding mode flight controller design for a quadrotor and the application in a heterogeneous multi-agent system," *IEEE Trans. Ind. Electron.*, vol. 64, no. 12, pp. 9389–9398, Dec. 2017.

[17] D. A. Mercado, R. Castro, and R. Lozano, "Quadrotors flight formation control using a leader-follower approach," in *Proc. Eur. Control Conf. (ECC)*, Zürich, Switzerland, Jul. 2013, pp. 3858–3863.

[18] M. F. B. Abas, D. Pebrianti, S. Azrad, D. Iwakura, Y. Song, K. Nonami, and D. Fujiwara, "Circular leader-follower formation control of quad-rotor aerial vehicles," *J. Robot. Mechtron.*, vol. 25, pp. 60–71, Feb. 2012.

[19] N. H. M. Li and H. H. T. Liu, "Formation UAV flight control using virtual structure and motion synchronization," in *Proc. Amer. Control Conf.*, Seattle, WA, USA, Jun. 2008, pp. 1782–1787.

[20] A. Abdessameud, I. G. Polushin, and A. Tayebi, "Motion coordination of thrust-propelled underactuated vehicles with intermittent and delayed communications," *Syst. Control Lett.*, vol. 79, pp. 15–22, May 2015.

[21] M. Turpin, N. Michael, and V. Kumar, "Trajectory design and control for aggressive formation flight with quadrotors," *Auto. Robots*, vol. 33, nos. 1–2, pp. 143–156, Aug. 2012.

[22] I. Bayezit and B. Fidan, "Distributed cohesive motion control of flight vehicle formations," *IEEE Trans. Ind. Electron.*, vol. 60, no. 12, pp. 5763–5772, Dec. 2013.

[23] D. Lee, "Distributed back-stepping control of multiple thrust propeller vehicles on balanced graph," in *Proc. 18th IFAC World Congr.*, Milan, Italy, Aug./Sep. 2011, pp. 8872–8877.

[24] W. Zhao and T. H. Go, "Quadcopter formation flight control combining MPC and robust feedback linearization," *J. Franklin Inst.*, vol. 351, no. 3, pp. 1335–1355, Mar. 2014.

[25] T. T. Ribeiro, A. G. S. Conceição, I. Sa, and P. Corke, "Nonlinear model predictive formation control for quadcopters," *IFAC-Papers OnLine*, vol. 48, no. 19, pp. 39–44, 2015.

[26] R. Wang and J. Liu, "Adaptive formation control of quadrotor unmanned aerial vehicles with bounded control thrust," *Chin. J. Aeronaut.*, vol. 30, no. 2, pp. 807–817, Apr. 2017, doi: 10.1016/j.cja.2017.01.007.

[27] S. Ariyibi and O. Tekinalp, "Modeling and control of quadrotor formations carrying a slung load," in *Proc. AIAA Inf. Syst.-AIAA Infotech@Aerosp.* Reston, VA, USA: American Institute of Aeronautics and Astronautics, Jan. 2018, p. 0250.

[28] R. Rafifandi, D. L. Asri, E. Ekawati, and E. M. Budi, "Leader–follower formation control of two quadrotor UAVs," *Social Netw. Appl. Sci.*, vol. 1, no. 6, p. 539, Jun. 2019, doi: 10.1007/s42452-019-0551-z.

[29] J. Ghommam, L. F. Luque-Vega, and M. Saad, "Distance-based formation control for quadrotors with collision avoidance via Lyapunov barrier functions," *Int. J. Aerosp. Eng.*, vol. 2020, 2020, Art. no. 2069631. [Online]. Available: https://www.hindawi.com/journals/ijae/2020/206963

[30] Y. Liang, Q. Dong, and Y. Zhao, "Adaptive leader–follower formation control for swarms of unmanned aerial vehicles with motion constraints and unknown disturbances," *Chin. J. Aeronaut.*, vol. 33, no. 11, pp. 2972–2988, Nov. 2020, doi: 10.1016/j.cja.2020.03.020.

[31] J. Estevez and M. Grana, "Improved control of DLO transportation by a team of quadrotors," in *Proc. Int. Work-Conf. Interplay Between Natural Artif. Comput. (IWINAC)*, in Lecture Notes in Computer Science, V. J. Ferrández, J. Álvarez-Sánchez, F. de la Paz López, J. T. Moreo, and H. Adeli, Eds., vol. 10338, 2017, pp. 117–126.

[32] J. A. Moreno and M. Osorio, "A Lyapunov approach to second-order sliding mode controllers and observers," in *Proc. 47th IEEE Conf. Decis. Control*, Cancún, Mexico, Dec. 2008, pp. 2856–2861, doi: 10.1109/CDC.2008.4739356.

[33] J. Yang, A. G. Thomas, S. Singh, S. Baldi, and X. Wang, "A semi-physical platform for guidance and formations of fixed-wing unmanned aerial vehicles," *Sensors*, vol. 20, no. 4, p. 1136, Feb. 2020, doi: 10.3390/s20041136.

[34] K. Máthé and L. Buşoniu, "Vision and control for UAVs: A survey of general methods and of inexpensive platforms for infrastructure inspection," *Sensors*, vol. 15, no. 7, pp. 14887–14916, 2015, doi: 10.3390/s150714887.

[35] S. Farí, X. Wang, S. Roy, and S. Baldi, "Addressing unmodeled path-following dynamics via adaptive vector field: A UAV test case," *IEEE Trans. Aerosp. Electron. Syst.*, vol. 56, no. 2, pp. 1613–1622, Apr. 2020, doi: 10.1109/TAES.2019.2925487.

[36] X. Wang, S. Roy, S. Farì, and S. Baldi, "The problem of reliable design of vector-field path following in the presence of uncertain course dynamics," *IFAC-PapersOnLine*, vol. 53, no. 2, pp. 9399–9404, 2020.

[37] J. C. Doyle, K. Glover, P. P. Khargonekar, and B. A. Francis, "State space solutions to standard H_2 and H∞ control problem," *IEEE Trans. Autom. Control*, vol. 34, no. 8, pp. 1228–1240, Nov. 1989.

[38] P. Gahinet and P. Apkarian, "A linear matrix inequality approach to H∞ control," *Int. J. Robust Nonlinear Control*, vol. 4, no. 4, pp. 421–448, 1994.

[39] C. Edwards and S. Spurgeon, *Sliding Mode Control: Theory and Applications*. London, U.K.: Taylor & Francis, 1998.

[40] W. Alam, A. Mehmood, K. Ali, U. Javaid, S. Alharbi, and J. Iqbal, "Nonlinear control of a flexible joint robotic manipulator with experimental validation," *Strojniški Vestnik-J. Mech. Eng.*, vol. 64, no. 1, pp. 47–55, 2018.

[41] F. Gouaisbaut, M. Dambrine, and J. P. Richard, "Robust control of delay systems: A sliding mode control design via LMI," *Syst. Control Lett.*, vol. 46, pp. 219–230, Jul. 2002.

[42] U. Javaid, A. Mehmood, A. Arshad, F. Imtiaz, and J. Iqbal, "Operational efficiency improvement of PEM fuel cell—A sliding mode based modern control approach," *IEEE Access*, vol. 8, pp. 95823–95831, 2020.

[43] S. A. Ajwad, J. Iqbal, R. U. Islam, A. Alsheikhy, A. Almeshal, and A. Mehmood, "Optimal and robust control of multi DOF robotic manipulator: Design and hardware realization," *Cybern. Syst.*, vol. 49, no. 1, pp. 77–93, Jan. 2018.

[44] Y. Feng, X. Yu, and Z. Man, "Non-singular terminal sliding mode control of rigid manipulators," *Automatica*, vol. 38, no. 12, pp. 2159–2167, 2002.

[45] J. J. E. Slotine and W. Li, *Applied Nonlinear Control*. Englewood Cliffs, NJ, USA: Prentice-Hall, 1991.

[46] V. K. Tripathi, A. K. Kamath, N. K. Verma, and L. Behera, "Fast terminal sliding mode super twisting controller for position and altitude tracking of the quadrotor," in *Proc. Int. Conf. Robot. Autom. (ICRA)*, May 2019, pp. 6468–6474.

[47] Y. Feng, X. Yu, and F. Han, "On nonsingular terminal sliding-mode control of nonlinear systems," *Automatica*, vol. 49, no. 6, pp. 1715–1722, Jun. 2013, doi: 10.1016/j.automatica.2013.01.051.

[48] X. Wang, E.-J. van Kampen, and Q. Chu, "Quadrotor fault-tolerant incremental nonsingular terminal sliding mode control," *Aerosp. Sci. Technol.*, vol. 95, Dec. 2019, Art. no. 105514, doi: 10.1016/j.ast.2019.105514.

[49] W. Wang and X. Yu, "Chattering free and nonsingular terminal sliding mode control for attitude tracking of a quadrotor," in *Proc. 29th Chin. Control Decis. Conf. (CCDC)*, May 2017, pp. 719–723.

[50] F. N. Martins and A. S. Brandão, *Motion Control and Velocity-Based Dynamic Compensation for Mobile Robots, Applications of Mobile Robots*, E. G. Hurtado, Ed. London, U.K.: IntechOpen, Nov. 2018. [Online]. Available: https://www.intechopen.com/books/applications-of-mobilerobots/motion-control-and-velocity-based-dynamic-compensationfor-mobile-robots, doi: 10.5772/intechopen.79397.

[51] C. Li, Q. Ren, F. Chen, and P. Li, "Vision-based formation control of a heterogeneous unmanned system," in *Proc. 45th Annu. Conf. IEEE Ind. Electron. Soc. (IECON)*, Oct. 2019, pp. 5299–5304, doi: 10.1109/IECON.2019.8927228.